Review

The Role of Perylene Diimide Dyes as a Cellular Imaging Agent and Enhancing Phototherapy Outcomes

Panangattukara Prabhakaran Praveen Kumar *

Posted Date: 10 March 2025

doi: 10.20944/preprints202503.0667.v1

Keywords: Perylene diimides; fluorescence; aggregation; cellular imaging; photothermal therapy; photodynamic therapy; chemotherapy

 doi:10.20944/preprints202503.0667.v1

Review

The Role of Perylene Diimide Dyes as a Cellular Imaging Agent and Enhancing Phototherapy Outcomes

Panangattukara Prabhakaran Praveen Kumar

Department of Biomedical Engineering and the Institute for Quantitative Health Science and Engineering, Michigan State University, East Lansing, MI 48824, USA; pananga1@msu.edu or p4praveen.18@gmail.com

Abstract: Recent advancements in phototherapy have underscored the need for effective cellular imaging agents that can enhance therapeutic efficacy and precision. Perylene diimide (PDI) dyes, known for their unique optical properties and biocompatibility, have emerged as promising candidates in this domain. This review paper provides a comprehensive analysis of the potential applications of PDI dyes in cellular imaging, specifically within the context of phototherapies. We explore the synthesis of these dyes, their photophysical characteristics, and mechanisms of cellular uptake. Moreover, this review highlights recent studies that demonstrate the effectiveness of PDI dyes in real-time imaging of cellular processes and their synergistic effects in photodynamic therapy (PDT) and photothermal therapy (PTT). By evaluating various experimental approaches and their outcomes, we aim to elucidate the advantages of employing PDI dyes in clinical settings. The findings of this review suggest that perylene diimide dyes are not only capable of enhancing imaging contrast but also optimizing the therapeutic response in targeted phototherapy applications. Ultimately, this paper advocates for further research into the integration of PDI dyes in clinical practice, emphasizing their potential to significantly improve patient outcomes in cancer and other diseases requiring photoactive treatment modalities.

Keywords: perylene diimides; fluorescence; aggregation; cellular imaging; photothermal therapy; photodynamic therapy; chemotherapy

1. Introduction

Perylene diimide (PDI) dyes have gained significant attention as versatile fluorescent probes and therapeutic agents due to their exceptional optical properties and tunable functionalities [1–3]. The unique chemical structure of PDIs, characterized by their strong absorption in the visible range and high quantum yield, positions them as ideal candidates for a variety of applications in cellular imaging and therapy [4,5]. In recent years, researchers have focused on leveraging PDIs for bioimaging, particularly emphasizing their role in live-cell imaging and targeted organelle visualization [6–8]. The ability to selectively stain specific cellular components enhances our understanding of cellular processes and facilitates the development of diagnostic tools in medical applications.

Moreover, PDIs are extensively explored in photodynamic therapy (PDT) and photothermal therapy (PTT) due to their ability to generate reactive oxygen species upon light activation, making them potent agents for cancer treatment [9,10]. The dual functionality of PDIs as imaging agents and therapy enhancers offers the potential for integrative approaches in cancer diagnosis and treatment, allowing for real-time monitoring of therapeutic efficacy and disease dynamics [6,11]. Additionally, the development of novel synthetic strategies has led to the functionalization of PDIs, improving their water solubility and biocompatibility, traits that are critical for biomedical applications [2,7,12].

Despite these advancements, several challenges hinder the widespread incorporation of PDIs in clinical settings. Key issues include the inherent low solubility of PDIs in aqueous environments, which limits their accessibility for biological applications [10,13]. Furthermore, addressing the aggregation phenomena that adversely affect the optical properties of PDIs in biological settings

 doi:10.20944/preprints202503.0667.v1

remains a major hurdle [14–16]. This aggregation can lead to reduced fluorescence intensity and imaging resolution, complicating cellular analysis [17,18].

This review aims to provide a comprehensive overview of the applications of perylene diimide dyes in cellular imaging and therapy. We will delve into recent advances in PDI-based systems, including their synthesis, modification, and application strategies, whilst critically examining the challenges that continue to pose obstacles in realizing their full potential in therapeutic and imaging techniques. Understanding and overcoming these challenges is fundamental for the future development of PDIs as effective tools in biomedical research and clinical practice.

2. General Synthetic Routes

Figure 1 illustrates the molecular structure of perylene-3,4,9,10-tetracarboxylic dianhydride (PTCDA), recognized as the foundational compound of this class [19,20]. Originally synthesized in the early 1910s, PTCDA serves as a precursor for various perylene diimide (PDI) dyes [21,22]. The figure also presents a generic PDI dye with labeled positions. Structural modifications, particularly at the imide N,N' sites and the hydrocarbon core's 1, 6, 7, and/or 12 positions (commonly referred to as “bay” positions), have led to PDIs with diverse chemical and physical properties.

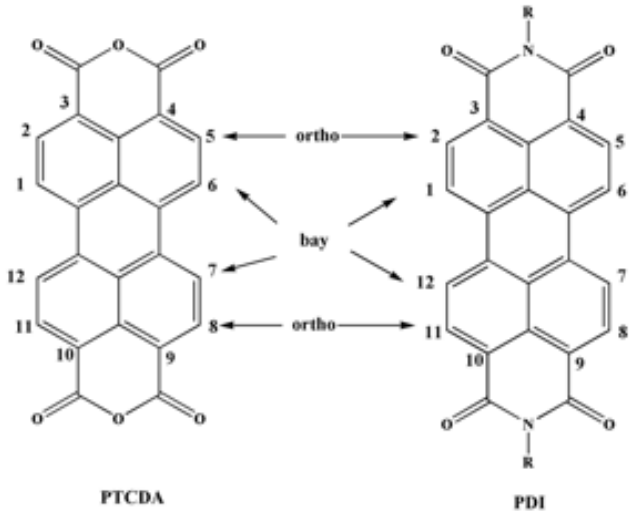

Figure 1. A generic chemical structure for PTCDA and PDI derivatives with the various positions in the chemical structure for functionalization.

2.1. Traditional Synthesis Methods

Traditionally, PDIs have been prepared through the "Langhals method," which entails reacting perylene-3,4,9,10-tetracarboxylic dianhydride (PDA) with primary amines in molten imidazole or qunoline at elevated temperatures, typically between 140 and 180 °C (Scheme 1, method A)[20,22,23]. Zinc acetate is frequently employed as a catalyst in this process, facilitating the formation of diimides under rigorous conditions with almost 95% yield for the products [24,25]. Despite its widespread use and reliability, this approach is associated with high energy demands and restricted compatibility with various functional groups due to the requirement for elevated temperatures. The standard procedure begins with dissolving PDA in molten imidazole, where primary amines are added to the reaction mixture [22]. Following the reaction, purification is typically carried out through filtration to isolate the formed PDIs, which are then washed to obtain final products priced for their high stability and excellent electronic properties.

An alternative approach involves treating PTCDA or its analogues, which have dibromo or tetrachloro substitutions at the “bay” positions, with primary amines in heated alcohols like n-butanol, carboxylic acids such as acetic or propionic acid, or alcohol-water mixtures like a 1:1 n-butanol/water system. This method has been shown to achieve isolated yields exceeding 90% (Scheme 1, method B) [26].

 doi:10.20944/preprints202503.0667.v1

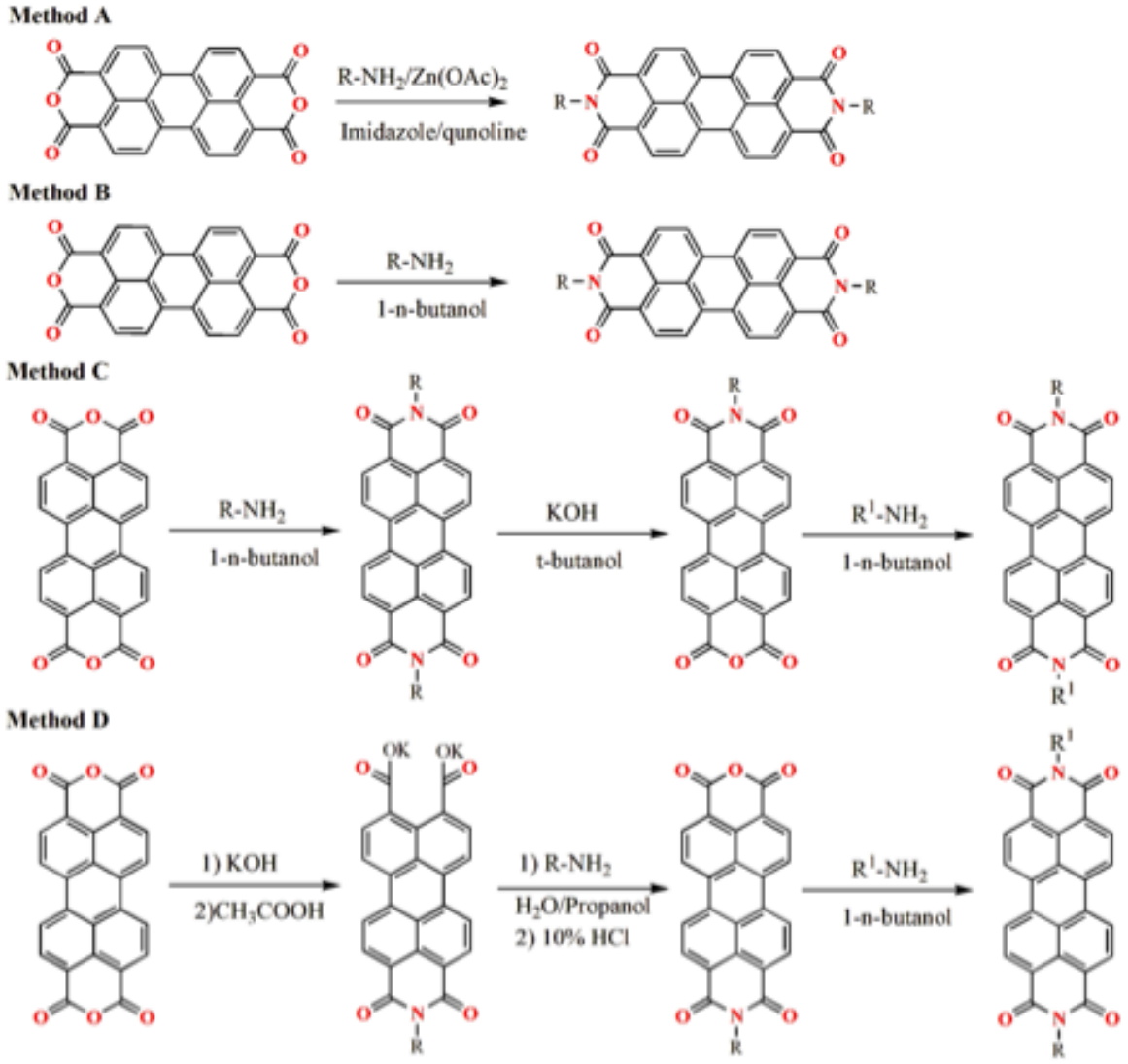

Scheme 1. Synthetic route for fabrication of dialkyl or diaryl PDI derivatives (method A-B). Method C and D represents the synthesis of asymmetrical PDI derivatives with different Substituents on Each Imide Position.

Unsymmetrical PDIs with distinct substituents at each imide position have been reported, though their direct synthesis from PTCDA remains challenging. Attempts involving the simultaneous or sequential addition of different amines often fail due to their varying reactivity with PTCDA, typically yielding only trace amounts of the desired product alongside predominant symmetrical PDIs. Consequently, multistep synthetic strategies are usually required. One approach (Scheme 1, method C) involves partial hydrolysis of symmetrical PDIs to generate perylene monoimide monoanhydride intermediates, which can then undergo imidization with a second amine or aniline to produce asymmetrical PDIs [26]. Another method utilizes mixed imide-anhydride intermediates, such as those reacted with o-phenylenediamine derivatives to form imide-benzoimidazole structures. However, direct imidization of PTCDA generally favors diimide formation due to the higher solubility of mixed imide-anhydride intermediates [27]. An alternative strategy, first introduced by Tam-Chan and colleagues in the late 1990s (Scheme 1, method D), involves partial hydrolysis of PTCDA to a mixed anhydride-dicarboxylate salt, followed by successive imidization steps [28]. Despite its effectiveness, method A is more commonly used due to its higher yield and simplified purification process [29–31].

 doi:10.20944/preprints202503.0667.v1

2.2. Room Temperature Synthesis

The development of a novel protocol allows for the synthesis of PDIs under much milder conditions at room temperature, addressing some of the environmental and efficiency issues seen with traditional methods. This method employs the reaction of PTCDA with aliphatic amines in solvents like DMF or DMSO, using dibutyldimethylammonium and K_2CO_3 as the base [32]. The process shows high conversions even at temperatures between 20 and 60 °C, presenting a significant advancement in the synthetic strategies for PDIs (Scheme 2, Method A). In this improved synthetic route, the reaction begins with the addition of the amine to a solution of PTCDA in DMF. Kinetic studies suggest that the formation of an amic acid intermediate occurs quickly, which subsequently transforms into the diimide via a slower intramolecular imidization. The advantage is that these reactions proceed under much less extreme conditions than previously utilized methods, resulting in higher functional group tolerance and less environmental impact.

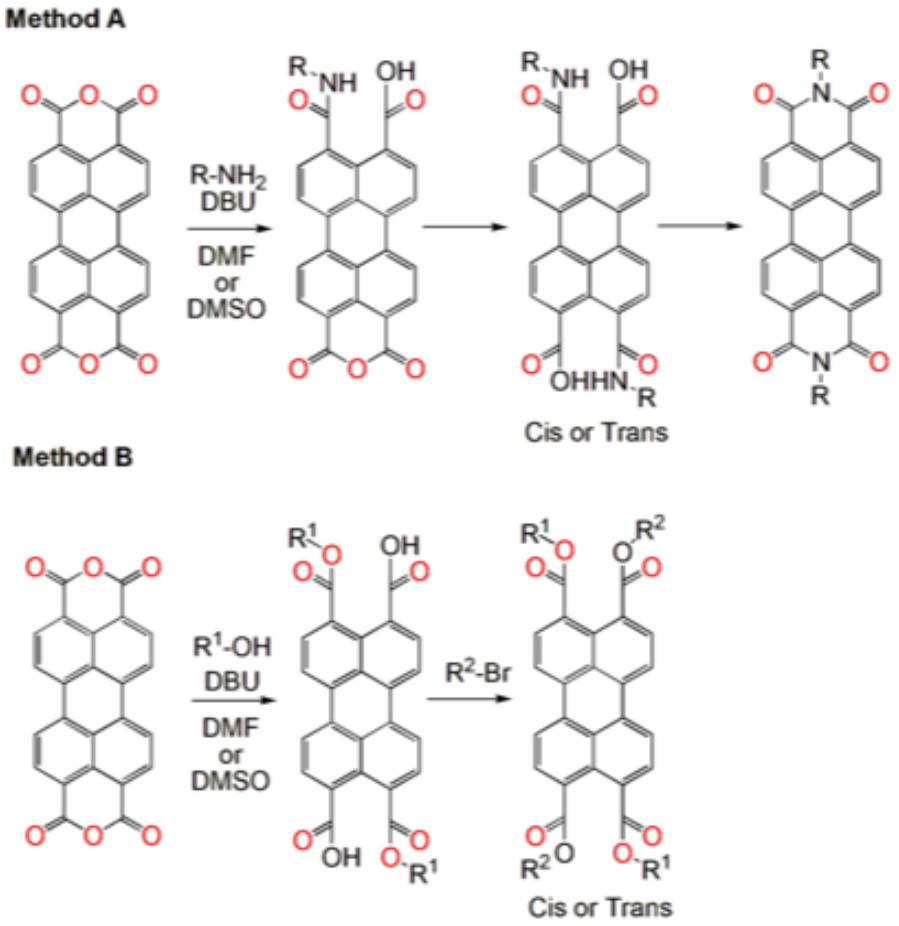

Scheme 2. Room temperature synthetic route for the fabrication of PDI derivatives. Method A showing use of amines and method B showing use of alcohols for the formation of PDI derivatives.

Compared to imidization, the esterification of PTCDA can occur under mild conditions, even at room temperature, as shown in Scheme 2, Method B [33,34]. In the initial step, an alcohol attacks the anhydride in the presence of the strong base DBU, leading to the formation of perylene-3,9-dicarboxylic acid-4,10-dicarboxylic dialkyl esters which exhibit high solubility. These intermediates then undergo a slower, rate-limiting reaction with an alkyl halide, ultimately yielding perylene-3,4,9,10-tetracarboxylic tetra-alkyl esters in nearly quantitative amounts. Notably, a modified approach has demonstrated the synthesis of an imide at room temperature, likely proceeding via an amic acid intermediate. Although this process involves a prolonged 3-day aminolysis reaction, making it less practical, it highlights the feasibility of PDI synthesis under mild conditions.

 doi:10.20944/preprints202503.0667.v1

2.3. Green Synthesis Approaches

In line with sustainability goals, recent methodologies have focused on greener synthesis techniques. One notable approach involves using a solvent-free method with a twin-screw extruder or employing water at high temperatures and elevated pressures. Although these methods require specific conditions, they showcase how PDI synthesis is evolving to reduce reliance on toxic solvents and harsh conditions [35,36]. Furthermore, a synthesis using K_2CO_3 in DMSO at 100 °C has demonstrated a green alternative, achieved quantitative yields while maintained the efficiency of the reaction. The incorporation of non-toxic solvents and bases is critical in this approach, contributing to the synthesis of PDIs that are environmentally friendly while retaining their essential qualities [32]. In one of the studies a series of PDI derivatives were prepared by hydrothermal reaction between alkyl amines and PTCDA [37,38]. A series of alkyl amines (n-C_n-NH_2; n = 3, 5, 18, 14) were treated with PTCDA derivative, and tetraethyl orthosilicate, and transferred the content into a non-stirred autoclave that was placed into an oven preheated at 200 °C for 24h. After cooling down the reaction, products were isolated by filtration to produce ultrapure PDI derivative with good optoelectronic properties [37].

2.4. Transition Metal-Catalyzed Methods

In recent years, synthetic methods utilizing transition metal-catalyzed couplings have gained attraction. For example, bay-substituted PDIs can be synthesized via C–C Suzuki coupling involving diaryl or brominated derivatives of PDIs, which ensures regioselectivity and potentially higher purity of the target compound [39–42]. Although this method opens new avenues for specific functionalization of the PDI core, challenges related to complex reaction conditions and post-reaction purification remain.

One of the most employed methodologies for synthesizing PDIs is the transition-metal-catalyzed Suzuki coupling reaction. This process utilizes palladium as a catalyst and facilitates the coupling of aryl or vinyl boronic acids with activated bromo or chloro derivatives of PDIs [43–45]. The advantage of this method lies in its ability to introduce functional groups at various positions on the PDI core, enhancing its solubility and electronic properties. For example, the synthesis of bay-substituted PDIs via mono- or dibromo PDI derivatives under Suzuki coupling conditions is well documented [39]. The successful incorporation of functional groups significantly alters the electronic character of PDIs, rendering them suitable for applications in organic photovoltaics and field-effect transistors.

Another effective transition-metal-catalyzed technique is the Stille coupling reaction, which involves the coupling of organotin reagents with PDIs [42,46–48]. This method allows the synthesis of complex PDI architectures that are otherwise challenging to obtain through traditional means. The Stille coupling reaction is celebrated for its selectivity and efficiency, leading to high yield syntheses of multiphenyl-substituted PDIs that display enhanced charge transport capabilities owing to the extended π-conjugation. The modification of PDI derivatives through these coupling reactions opens avenues for tailoring their absorption characteristics and energy levels, aligned with specific applications in organic electronics.

Transition metal-catalyzed C–H activation has also proven to be a revolutionary approach in PDI synthesis, enabling the direct functionalization of C–H bonds in the PDI core [40,49,50]. Such strategies diminish the need for prefunctionalized substrates, streamlining the synthesis process. This technique has been particularly advantageous for constructing PDIs that incorporate diverse functional groups, thus enhancing the versatility of their applications. The activation of C–H bonds require precise coordination and catalyst design to achieve selective reactivity, contributing to the development of advanced perylene derivatives with tailored electronic properties.

3. Photophysics of PDIs

PDIs display well-defined absorption and emission spectra, with emission peaks typically appearing at wavelengths that are mirror images of their absorption bands. The structural integrity of PDIs allows for the fine-tuning of their optical properties through chemical modifications, such as

 doi:10.20944/preprints202503.0667.v1

substituents on the perylene core. PDIs exhibit strong and broad absorption spectra, typically found in the UV-visible region. The absorption peaks generally occur around 530 nm to 550 nm, which corresponds to the π-π* electronic transitions of the conjugated perylene core. The ability of PDIs to absorb light efficiently is largely due to their planar structure and extensive π-conjugation, which allows for effective overlap of π-orbitals among adjacent molecules. Substituent groups on the PDI core can considerably alter the absorption characteristics. As demonstrated in studies, the presence of different substituents can shift the maximum absorption bands. For example, one study reported shifts in the maximum absorption bands for various **PDI (1-3)** derivatives, with observed ranges of 555 nm to 585 nm contingent upon specific molecular modifications (Figure 2A,B) [51]. Such shifts significantly affect the electronic transitions within the molecule and highlight the tunability of PDIs for tailored applications. Additionally, the aggregation of PDIs can lead to significant changes in their absorption and emission spectra (Figure 2B). When PDIs aggregate, for example, due to increased concentration or structural interactions, the UV-visible absorption profiles exhibit alterations, primarily due to H-aggregate formation. Such aggregation phenomena can lead to altered intensities and band shifts in the absorption spectra, essential for understanding their behavior in solid-state applications [52,53].

The emission properties of PDIs are significantly influenced by the nature and position of substituents on the perylene core [54,55]. PDIs are celebrated for their high luminescence efficiency, excellent thermal stability, and tunable optical properties, making them suitable for applications in organic electronics, photovoltaic devices, and fluorescent materials. This review explores how different substituents modulate the emission characteristics of PDIs, focusing on the mechanisms by which they alter photophysical properties including absorption, fluorescence intensity, and emission wavelengths. The optical properties of PDIs are highly dependent on the electronic interaction between the PDI core and the substituents. Substituents can affect the energy levels of the highest occupied molecular orbital (HOMO) and the lowest unoccupied molecular orbital (LUMO), thereby influencing the absorption and emission spectra. Electron-donating groups typically lead to red shifts in the absorption and emission spectra due to increased conjugation with the perylene core [56]. PDIs with electron-donating substituents such as phenoxy and chlorophenoxy groups, the introduction of these substituents has been shown to stabilize the excited states, facilitating higher fluorescence efficiencies. The effect is particularly pronounced when such substituents reduce the energy gap between the HOMO and the LUMO levels, leading to enhanced light absorption and subsequent emission. Conversely, electron-withdrawing substituents can induce blue shifts due to decreased electron density in the conjugated system.

The introduction of bulky substituents can also hinder intermolecular π-π interactions, which are known to cause aggregation-caused quenching (ACQ) in solid-state PDIs. The modification of PDIs by substituents at the bay position (the positions adjacent to the carbonyl groups) has demonstrated profound effects on their self-assembly and fluorescence-quenching characteristics [57–59]. For instance, **PDI-(4- 7)** derivatives with unsymmetrical substituents show distinct emission spectra indicative of their unique packing structures (Figure 2C,D) [57]. The fluorescence efficiency of PDIs is a major contributing factor to their utility in electronic and optoelectronic devices. PDIs typically exhibit high fluorescence quantum yields, often approaching unity in diluted solutions, which however can significantly decrease upon aggregation in solid states due to ACQ. For instance, studies reveal that while the emission quantum yield of certain PDIs in solution can be as high as 57.2%, the yield notably drops to 6.2% in their solid state [51]. This disparity exemplifies the critical importance of molecular aggregation and the influence of environmental conditions on fluorescent properties.

Recent advances in the design of PDIs with various substituents have yielded materials with tailored photophysical properties suitable for specific applications. For example, structural modifications can be optimized for enhanced photothermal conversion or fluorescence properties, which are essential for the development of advanced electronic and photonic devices [11]. Moreover, the solubility and aggregation behavior of PDIs in different environments are also influenced by substituents. The flexibility imparted by certain substituents can mitigate aggregation propensity in solvents, enabling higher fluorescence yields in solution states, while rigid substituents lead to well-

 doi:10.20944/preprints202503.0667.v1

defined nanostructures but can enhance self-quenched emission in solid states [60]. This balance between solubility and optical performance is critical in applications ranging from organic light-emitting diodes to solar cells.

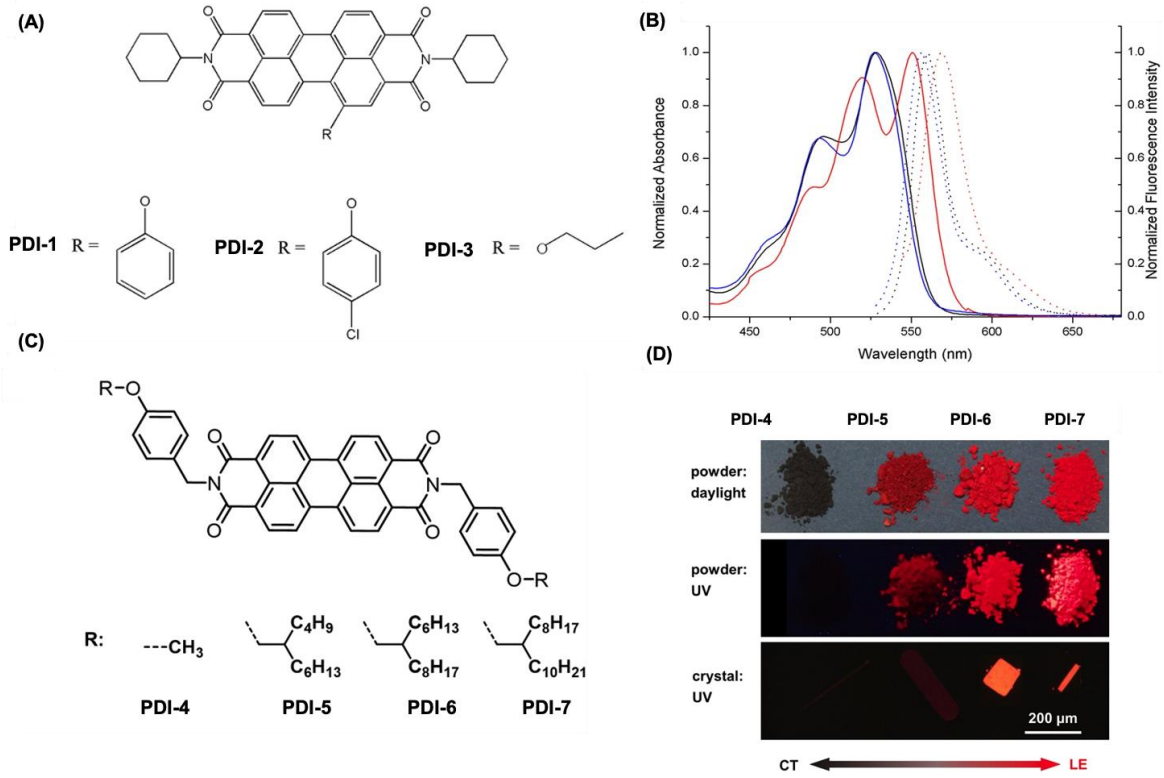

Figure 2. Structure and optical properties of various PDI derivatives. (A) Molecular structure and (B) Absorption spectra (solid lines) and corresponding fluorescence spectra (dot lines) for **PDI (1-3)** with Bay substitutions with various substituents. **PDI-1** (black), **PDI-2** (blue) and **PDI-3** (red) in DCM. (C) Chemical structures of alkoxybenzyl-substituted **PDI-(4-7**). (D) Photographs showcase the corresponding powders under daylight and UV irradiation (365 nm), along with fluorescence images of single crystals captured with a 158-millisecond exposure time [51,57].

4. Synthesize of Water Soluble PDI Derivatives

PDIs face significant challenges in biological and medicinal applications due to their poor water solubility, weak fluorescence in aqueous environments, and strong tendency to aggregate, which stems from intrinsic π–π stacking interactions between perylene backbones [52,61]. To overcome these limitations, extensive research has focused on enhancing the water solubility of PDIs by incorporating hydrophilic groups at the bay region, imide positions, or ortho-positions. One approach involves the direct integration of ionic groups, such as cationic ammonium salts, anionic carboxylic acids, sulfonic acids, and phosphonic acids, into the perylene chromophore, resulting in water-soluble PDIs. Another effective strategy is the attachment of non-ionic substituents containing multiple polar groups, including poly (ethylene glycol) (PEG), polyglycerol (PG) dendrons, and dendritic carbohydrate derivatives, at these key positions. These modifications help prevent aggregation of the perylene cores, leading to PDIs with enhanced fluorescence and high fluorescence quantum yields in aqueous solutions. Ionic and non-ionic groups such as $–SO_3H$, –OH, $–NH_2$, –NHR, –COOH, –O– can be introduced into the bay or ortho positions of PDIs to improve their water solubility and in turn for various applications.

4.1. Substituting with Anionic Groups

Various anionic groups such as carboxylic, sulphonic, phosphonic acid groups can be introduced into the PDI back bone to improve their solubility in water and in biological media. As shown in

 doi:10.20944/preprints202503.0667.v1

Figure 3, a series of PDI derivatives was prepared by Mullen and coworkers by substituting the bay and imide positions of parent PTCDA derivative [62–64]. As shown in Figure 3, **PDI-8,** featuring four carboxylate sodium salts in the bay-region, was synthesized by reacting the parent acid with sodium hydroxide, enhancing water solubility. However, its chromophore with carboxyl groups remains water insoluble. The **PDI-9** derivative with four sulfonic acids, exhibited a solubility of 8.0×10^{-2} mol L^{-1}. Reducing hydrophilic groups from four to two lowered both solubility and fluorescence quantum yield in **PDI-9** derivative (FQY = 12%). The monofunctional **PDI-10** had similar solubility to ionic PDIs and retained a carboxyl handle for further modifications. **PDI-9** showed an FQY of 58%, reduced from 100% in organic solvents due to aggregation, vibrational relaxation, and photo-induced electron transfer. Whereas **PDI-8** had a lower FQY (7%) due to lipophilic alkyl spacers, while **PDI- 11s** FQY was slightly lower (49%) than **PDI-9**, as imide substitution influenced fluorescence. **PDI-12**, with ortho-phosphonic acids, exhibited resistance to aggregation and quenching, achieving an FQY of 77% and was successfully used for HeLa cell labeling. Akkaya et al. synthesized green PDI dyes (**13a–c**) with dialkylamino groups, where **13c** efficiently generated singlet oxygen under red light, showing cytotoxic effects [65]. Malik et al. developed chiral PDIs (**14a–b**) with aspartic acid at imide positions, forming reddish-brown hydrogels at pH 4 [66]. Upon drying, these hydrogels produced helical fibers stabilized by π–π stacking and hydrogen bonding.

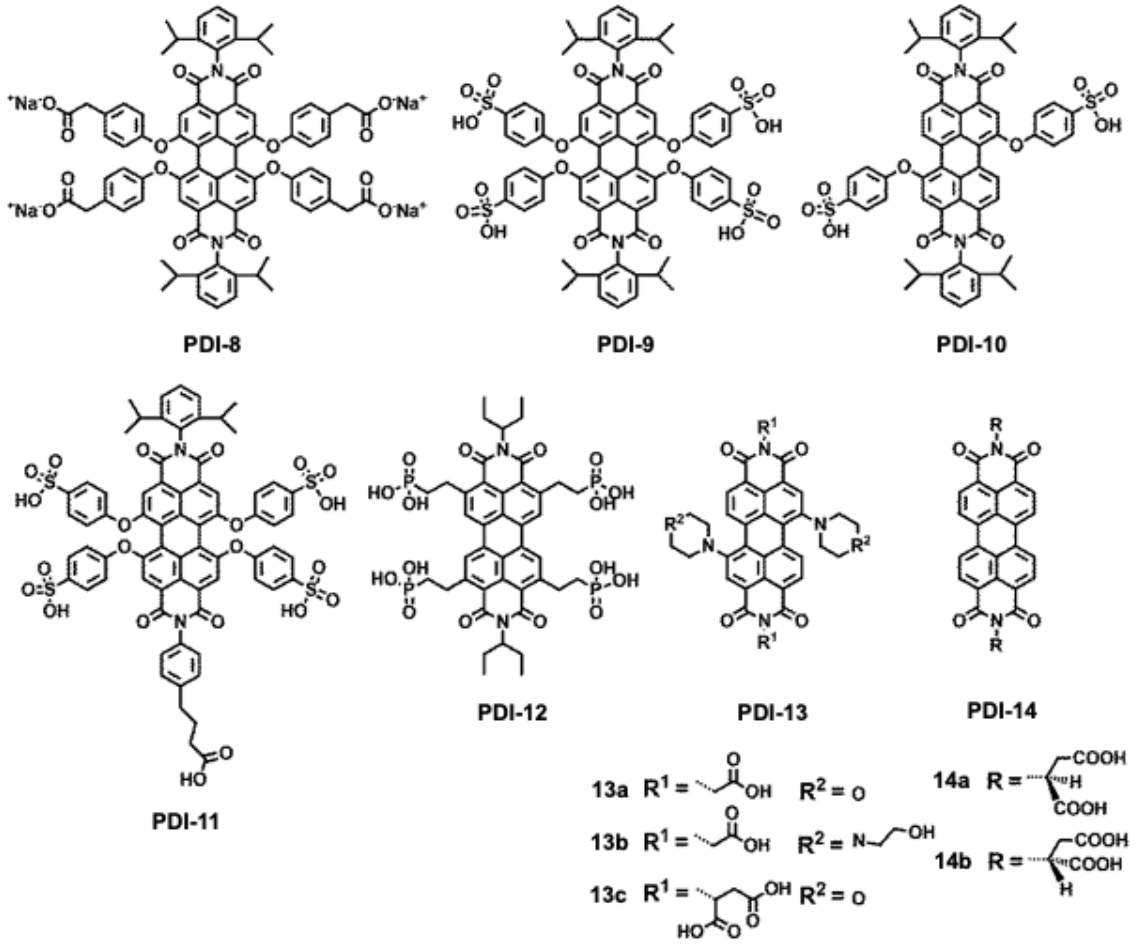

Figure 3. Chemical structures for water soluble PDI derivatives (**8-14**) having anionic charges on various positions.

Given the vast potential of water-soluble PDIs in biosensing and metal ion detection in aqueous environments, Kozma et al. synthesized four novel amino acid-based **PDIs (15-18**): PDI-Thr (L-threonine, **PDI-15**), PDI-Asp (L-aspartic acid, **PDI-16**), PDI-Met (L-methionine, **PDI-17**), and PDI-Cys. (L-cysteine, **PDI-18**) as shown in Figure 4A [67]. Notably, PDI-Thr and PDI-Cys have not been previously reported. This study provides a comparative analysis of their aggregation behavior in both organic and aqueous media using absorption and emission spectroscopy. The incorporation of

 doi:10.20944/preprints202503.0667.v1

amino acid carboxyl groups at the peripheral nitrogen atoms ensures solubility in aqueous solutions at pH ≥ 6, while their aggregation tendencies are influenced by the specific amino acid side chain. By examining their optical properties in DMSO and buffered aqueous solutions, the study highlights their concentration-dependent self-association, paving the way for the development of innovative PDI-based sensing platforms (Figure 4B).

Heek et al. fabricated polyglycerol dendronized PDI derivatives (**19-22**) with different generation of dendrons such as G1-PDI-G1 (**PDI-19**), G2-PDI-G2 (**PDI-20),** G3-PDI-G3 (**PDI-21**), and G4-PDI-G4 (**PDI-22**) with excellent water solubility (Figure 4C) [68]. The highly sterically demanding dendron substituent resulted in a dye with an exceptional fluorescence quantum yield nearing 100% in water for the lowest concentration such as 10^{-7} M (Figure 4D). This confirms that no specific quenching mechanism, such as excited-state proton transfer, is active in this class of fluorophores. Consequently, core-unsubstituted PDIs can exhibit strong fluorescence in water when aggregation is effectively prevented, paving the way for diverse applications in fluorescent labeling and sensing.

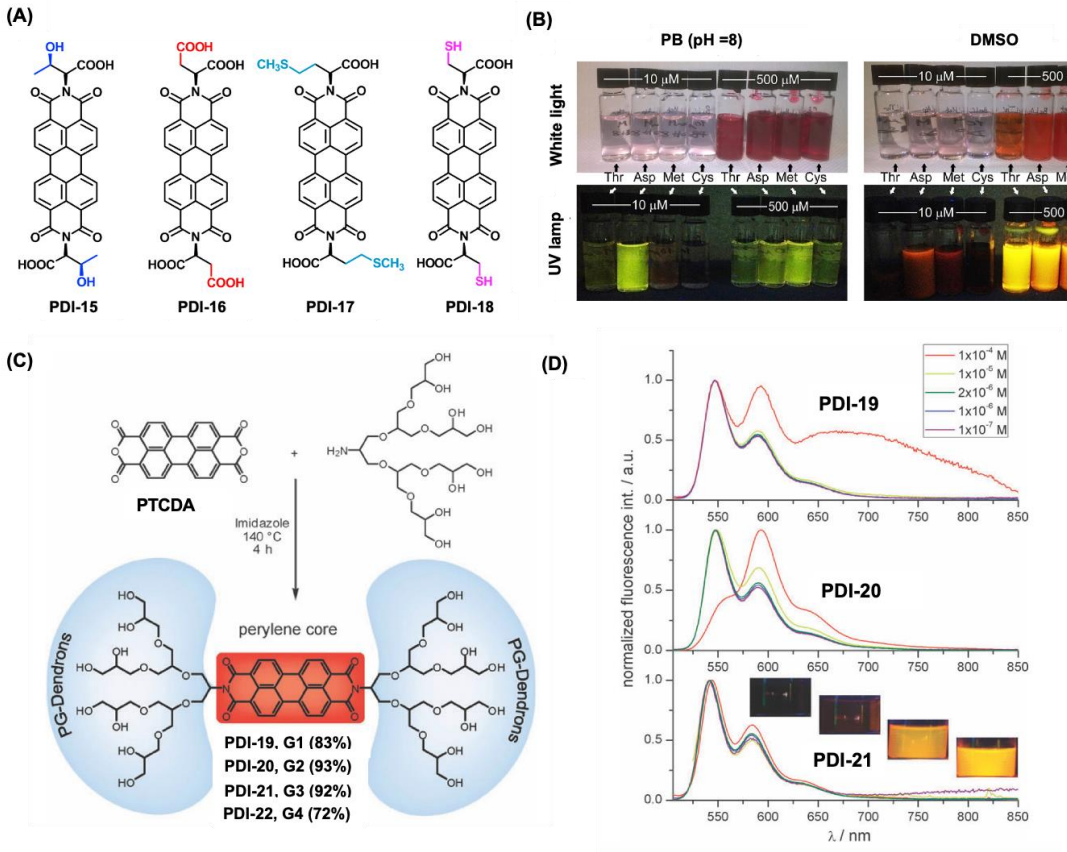

Figure 4. Chemical structures for various water soluble PDI derivatives with anionic groups on imide positions. (A) Molecular structures of the PDIs functionalized with aminoa cids. PDI-Thr (L-threonine, **PDI-15**), PDI-Asp (L-aspartic acid, **PDI-16**), PDI-Met (L-methionine, **PDI-17**), and PDI-Cys. (L-cysteine, **PDI-18**). (B) A visual comparison of the four amino acids functionalized PDI derivatives in PBS and DMSO at two concentrations, observed under white light and UV illumination (λ = 365 nm). (C) Synthetic scheme for the polyglycerol functionalized PDI derivatives (**19-21**), and showing the structure for **PDI-20**. (D) The fluorescence measurements of **PDI-19** (top), **PDI-20** (middle), and **PDI-21** (bottom) were recorded across concentrations ranging from 10^{-4} M to 10^{-7} M with an excitation wavelength of 490 nm. The inset displays a photograph of PDI solutions (**19–21**, labeled [G1]–[G4] from left to right) under UV-light illumination at a concentration of 1.43×10^{-4} M. [67,68].

Yin et al. described negatively charged fluorescent core–shell macromolecules (**22**,**23**, and **24**) featuring a central PDI chromophore enclosed by hydrophobic polyphenylene dendrimers and flexible polymer shells [69–71] . Unlike polyamide dendrons, polyphenylene dendrimers are bulkier and more rigid, effectively preventing aggregation and protecting the inner perylene chromophores.

 doi:10.20944/preprints202503.0667.v1

The outer polymer layers, enriched with carboxylic acids via atom transfer radical polymerization enhance water solubility and charge density. **PDIs-22** and **23**, classified as 1G dendrimers, contain eight arms with carboxylic acids and sodium salts, while **PDI-24**, a 2G analogue, has sixteen arms. These macromolecules exhibit high water solubility (>10 g/L). Fluorescence quantum yields (FQYs) are 13% for **PDI-22** and 22% for **PDI-24** in water. Additionally, **PDI-22** (n = 55) self-assembles into unimolecular fluorescent polymeric micelles in aqueous media, with pH-dependent size and fluorescence due to its polyelectrolytic outer shell. These PDI derivatives used for nuclear staining and for the detection of DNA.

4.2. Substituting with Cationic Groups

PDI derivatives can be made water soluble by substituting them with quaternary ammonium salt or converting nitrogen into its protonated form. As shown in Figure 5A, Yu et al. fabricated a cationic **PDI-23**, derivative with two positive charges on the imide nitrogen back bone and showed a water solubility for concentration greater than 30 mM [72]. Owing to the positive charges in the backbone the repulsive forces tend them not to aggregate in aqueous media. This PDI derivative showed good turn- on fluorescence with aptamer-binding proteins. A series of water soluble cationic **PDI-24a-f** derivatives was prepared by Yin et al (Figure 5A) [73]. These PDI dyes showed cancer cell growth suppression due to their positive charges, and they act as DNA intercalators. **PDIs-24c** and **24f**, which incorporate quaternary ammonium cations, demonstrate significantly enhanced water solubility (> 10 g/L) compared to **PDIs 24a** and **24d,** which contain primary ammonium salts and exhibit much lower solubility (approximately 2 g/L). The fluorescence quantum yields of **PDIs 24a–24f** vary, measuring 1.1%, 22.8%, 26.2%, 4.7%, 5.6%, and 25.3%, respectively. Among these, **PDI-24b** shows minimal cytotoxicity, maintaining 90% cell viability in non-cancerous cells. Additionally, **PDIs 24d, 24e**, and **24f** have a unique ability to selectively accumulate in cell nuclei by interacting with DNA through intercalation and electrostatic forces (Figure 5B).

In of the studies two water-soluble PDI-cored star polycations, **25** and **26** were synthesized via atom transfer radical polymerization with distinct amines at the PDI bay region [74]. These polymers feature a fluorescent PDI core with PAEMA (**25**) or PDMAEMA (**26**) arms, enhancing water solubility through polar functional groups (Figure 5C). Both exhibit concentration-dependent absorption in aqueous solutions while remaining as single molecules (7.26–28.9 mM). With an emission peak at 622 nm and fluorescence quantum yields of 14% (**PDI-25**) and 6% (**PDI-26**), they are suitable for fluorescence detection and live-cell imaging. Their high zeta potentials (37.8 and 56.5) allow electrostatic DNA interactions and possess high cell uptakes (Figure 5D). Gryszel et al. fabricated a PDI derivative with two quaternary ammonium salts at imide position, which act as a catalyst for the light-induced conversion of dissolved oxygen to hydrogen peroxide [75]. Even though this dye showed promising light absorption property, the quantum efficiency of photon-to-peroxide conversion remains low, <1 % quantum efficiency. While this molecular method may not be the most efficient for producing peroxide through photosynthesis from dissolved oxygen, it shows great potential for applications in biotechnology and biophysics. Bag et al. studied solvent dependent emission properties for a cationic PDI derivative. The experiments were performed using water miscible solvents such as ethanol, DMSO, THF etc [76]. Experimental and theoretical studies showed these dyes showed enhanced emission in the monomeric and in the assembled H-aggregate states. An enhancement in emission was observed for ethanol/water system due the favorable enthalpic contribution.

 doi:10.20944/preprints202503.0667.v1

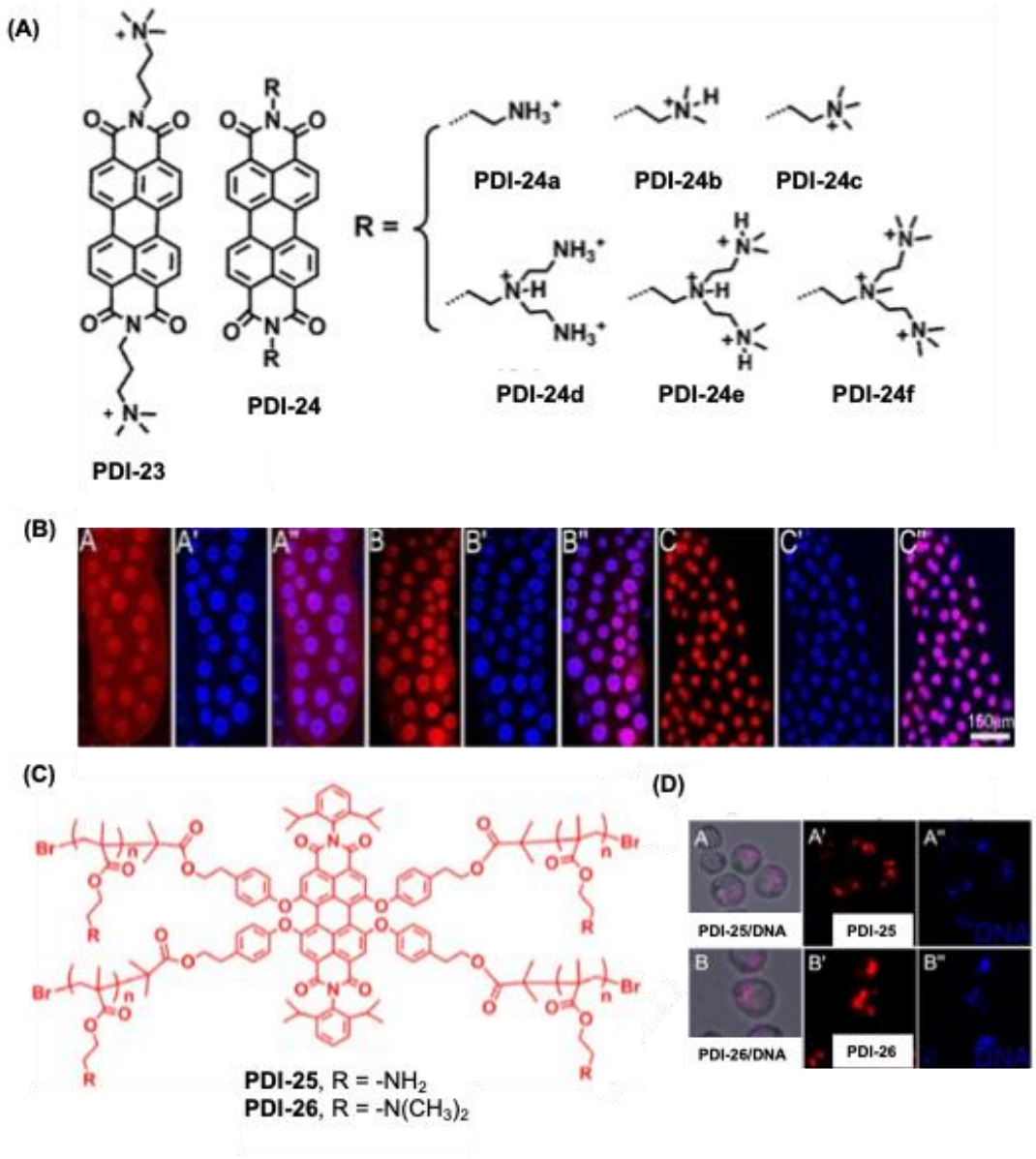

Figure 5. Chemical structures for various water soluble PDI derivatives with cationic groups on imide positions and bay positions. (A) Chemical structures for PDI derivatives **PDI- 23-24**. (B) Fluorescence images of salivary glands incubated with (A, B, and C) PDIs 24d, 24e, and 24f (red), (A′, B′, and C′) DAPI (blue), and (A″, B″, and C″) merged channels of PDIs **24d–24f** and DAPI. (C) Structure for the Structures of (PAEMA, **PDI-25**) and (PDMAEMA, **PDI-26**). (D) Fluorescence images of (A) **PDI-25**/DNA and (B) **PDI-26**/DNA complexes internalized into cells after 48 h incubation (N/P = 20). A′ and B′ are fluorescence images of **PDI-25** and **PDI-26** (red). A″ and B″ are fluorescence images of DNA labeled with CXR Reference Dye (blue) [72–74].

Yin and colleagues reported the synthesis of a series of water-soluble, cationic dendrimers featuring a perylene diimide (PDI) core through a ‘‘click’’ reaction (**PDI-27a-c**) [77]. The fluorescent PDI core facilitates cellular uptake tracking via fluorescence microscopy. The dendrimers possess peripheral primary amines, which acquire positive charges upon hydrochloric acid treatment, contributing to their solubility. The outer cationic structure effectively prevents PDI aggregation by leveraging steric hindrance and electrostatic repulsion. Additionally, the presence of multiple polar groups (–OCO– and –S–) further enhances water solubility, exceeding 10 g/L. These dendrimers exhibit excellent photostability, and their absorbance, fluorescence intensity, and fluorescence quantum yields (9%, 12%, and 25%) increase with dendrimer generation. Moreover, their cytotoxicity remains low, with cell viability exceeding 90% at 6 μM concentration.

 doi:10.20944/preprints202503.0667.v1

4.3. PDI Derivatives with Non-Ionic Substituents

Non-ionic groups such as polyethylene glycol (PEG), polyglycerol (PG) dendrons, and dendritic carbohydrates can be substituted to make water soluble PDIs for various applications. Such groups render the π-π stacking interaction of PDI core retaining their emissive properties. As shown in Figure 6A a series of PDI-cored PEG dendrimers **PDI-28a-c** were prepared. The branched PEG and poly glutamic acid groups suppress the aggregation of **PDI** with an improved water solubility for the core[78]. **PDI-28a**, containing 0G dendrons, remains aggregated across its tested concentration range (1×10^{-6} to 1×10^{-4} M), as indicated by a broad absorption spectrum, a hypochromically shifted absorption maximum, and low fluorescence efficiency (4%) (Figure 6B). In contrast, higher dendron generations in dyes **PDI-28b** and **PDI-28c** introduce steric hindrance, enhancing PDI hydrophilicity and significantly increasing their fluorescence quantum yields in water (65% and 93%) due to complete suppression of aggregation. MTT assay results confirm that **PDIs 28a–c** exhibits minimal cytotoxicity (over 90% cell viability), as PEG chains prevent unwanted interactions with extracellular proteins.

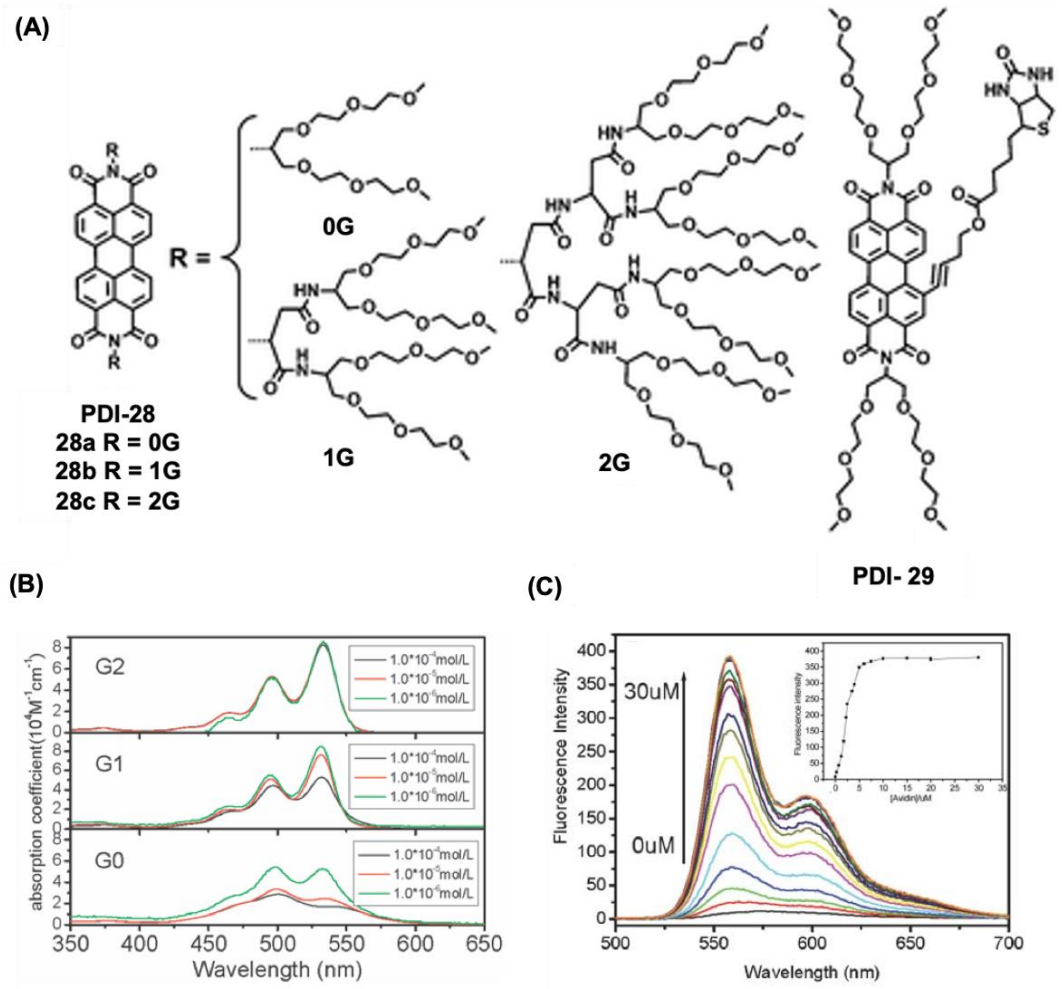

Figure 6. (A) Chemical structure for PDI derivatives 28-29 with PEG water soluble groups on backbone. (B) Concentration dependent absorption spectra for **PDI-28a-c**. (C) The fluorescence spectrum of **PDI-29** (10 μM) exhibits changes upon incremental addition of avidin (0–30 μM), with the inset displaying the corresponding fluorescence titration curve [78,79].

Additionally, the development of bay-substituted **PDI-29**, modified with a biotin ligand, allows for the formation of highly stable self-assembled nanostructures in aqueous media, leading to total fluorescence quenching (Figure 6A). Whereas on interaction with avidin the probe showed a tun-on fluorescence for tracking the targeted proteins in living cells (Figure 6C).

 doi:10.20944/preprints202503.0667.v1

The introduction of functional groups in the bay-region of PDIs induces a red shift in the absorption maximum and enhances the Stokes shift, reducing phototoxicity and biological auto-fluorescence interference. Zimmerman and colleagues developed neutral, water-soluble **PDIs** (**30-32**) with bay-substituted amide-coupled PG dendrons, which provide steric hindrance to minimize π–π interactions (Figure 7A) [80]. Compounds **32b** and **32c** were synthesized through click reactions between monofunctional **32a** and alkyne-functionalized biotin and maleimide. These PDIs exhibit high fluorescence quantum yields (FQYs) in water (57%–83%), influenced by encapsulation efficiency. **PDI-31**, with extensive dendron substitution, achieves the highest FQY (83%) due to superior solubilization. However, intramolecular crosslinking of dendronized PG reduces hydroxyl groups, leading to decreased aqueous solubility and FQY.

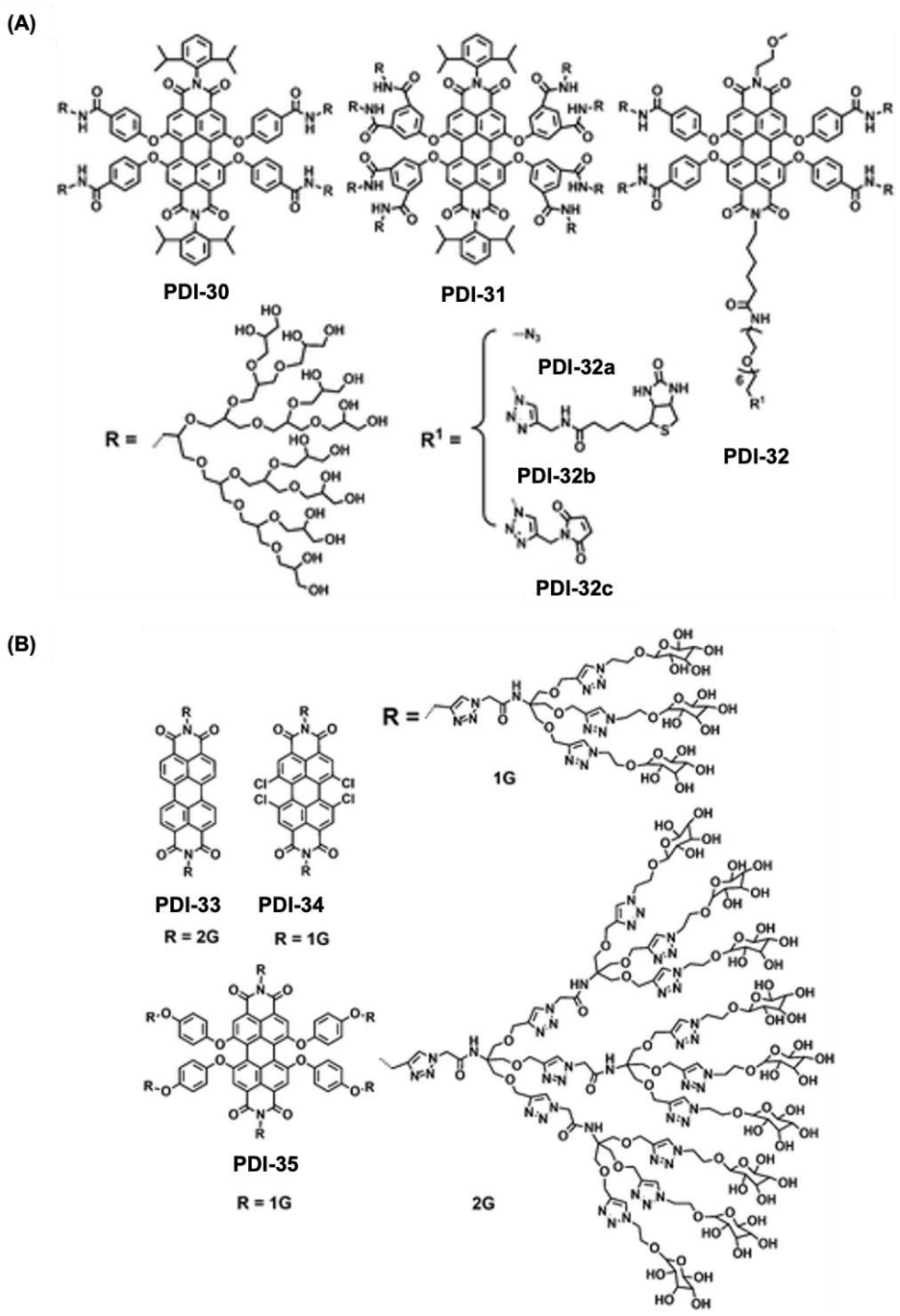

Figure 7. (A) Chemical structure for the PDI derivatives **PDI- 30-32** having polyglycerol dendrons in the bay region. (B) Chemical structure for PDI based glycodendrimers (**PDI-33-35**).

 doi:10.20944/preprints202503.0667.v1

A series of water-soluble **PDIs-33–35** modified with glycodendrimers at the imide-positions or bay-region were synthesized using a click reaction followed by deprotection (Figure 7B). Their UV-vis spectra show a transition from monomeric to aggregated states as concentration increases and temperature decreases, indicating aggregation dependence. At low concentrations (5.0×10^{-6} M), the FQYs of **PDI-33** and **PDI-36** are 59.9% and 54%, respectively, but fluorescence diminishes with increasing concentration due to aggregation. **PDI-35**, with glycodendrimers at both positions, exhibits minimal fluorescence due to intramolecular electron transfer. MTT assays confirm that **PDI-33** is non-cytotoxic, maintaining 110% cell viability at 50 μg/mL.

5. Biomedical Application of PDI

Water-soluble perylene diimide (PDI) derivatives have garnered substantial attention in recent years due to their unique optical properties, biocompatibility, and potential for versatile applications in biological systems [1,81,82]. The modification of PDIs to enhance their water solubility has led to significant advancements in various biomedical applications, including photodynamic therapy (PDT) [9,83], biosensing [84,85], imaging [86,87], and drug delivery[88–90].

5.1. Biosensing Applications

The fluorescence properties of water-soluble PDIs make them ideal candidates for biosensing applications, enabling the detection of various analytes, including ions, small molecules, and biomolecules [81,82]. Their high quantum yields and photostability allow for sensitive and real-time monitoring in biological environments. PDI-based sensors have been designed for multiple applications, including pH monitoring [3,91,92], metal ion detection [1,93] , and biomolecular recognition [94–96].

Yin et al. reported fluorescent nanotubes formed by electrostatic interactions between oppositely charged molecules (**PDI-34** and **PDI-35**) as DNA biosensors (Figure 8A) [70]. The positively charged component (**PDI-34**) adhered to surfaces and bound negatively charged DNA, enhancing fluorescence intensity by stabilizing the central PDI chromophore in solution. Later, the team developed a highly sensitive and selective DNA sensor using energy transfer between a negatively charged donor (**PDI-35;** Figure 8A) and Cy5-labeled DNA as the acceptor [97]. Excitation at 543 nm facilitated energy transfer, significantly amplifying the fluorescence signal, enabling ultrasensitive DNA detection.

Yan developed the ATP sensor **PDI-36** by modifying it with a Zn^{2+}–DPEN moiety at its imide positions (Figure 8B) [84]. The sensing mechanism relies on ATP binding to the two Zn^{2+} centers, leading to a significant fluorescence enhancement in aqueous solution. Other phosphate-containing anions were tested, but none exhibited a similar fluorescence response, highlighting the sensor's high selectivity for ATP. Li introduced another fluorescence-based sensing approach using **PDI-37** in combination with Cu^{2+} ions (Figure 8C) [98]. The **PDI-37**/Cu^{2+} complex (1:2) forms aggregates in aqueous solution, causing fluorescence quenching. Upon the addition of pyrophosphate (PPi), competitive binding with Cu^{2+} disrupts these aggregates, restoring fluorescence. This selective fluorescence "turn-on" mechanism enables sensitive PPi detection with a limit of detection (LDL) of 0.2 μM (Figure 8D). Expanding on this concept, Iyer developed a nanocomposite sensor composed of histidine-functionalized PDI derivative, graphene oxide, and Cu^{2+} [95]. The PCG system operates via the same fluorescence recovery mechanism and is capable of detecting PPi in aqueous environments, including physiological conditions and living cells. The sensor exhibits high sensitivity with an LDL of 60 nM, attributed to the strong interaction between the Cu^{2+}-PDI complex and PPi. Additionally, the sensor was adapted for solid-phase applications by integrating it with PVA hydrogel films and thin-layer chromatography plates, enhancing its practical usability. Sukul further refined this detection strategy by designing PDI–Cu^{2+} aggregates, which display sequential fluorescence responses [96]. The addition of Cu^{2+} leads to fluorescence quenching, while subsequent PPi binding restores fluorescence. This system demonstrates high selectivity for Cu^{2+} and PPi over other phosphate species, including AMP, ADP, and ATP. Notably, the PPi detection can be visually observed through a color change in the solution, offering a simple and effective detection method with a limit of detection of 0.11 μM.

 doi:10.20944/preprints202503.0667.v1

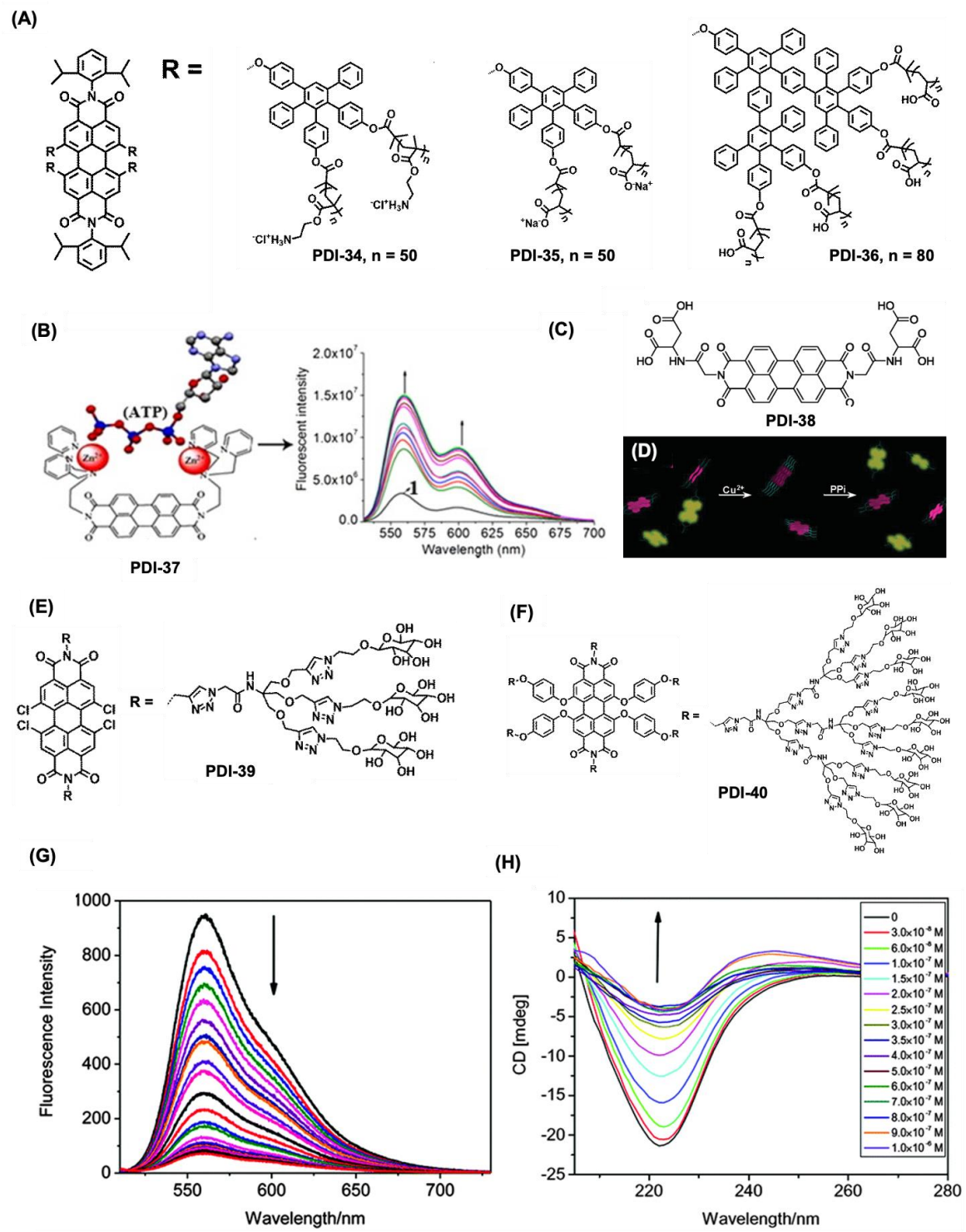

Figure 8. PDI derivatives for biosensing applications. (A) Chemical structure for **PDI-34-36** used for the detection DNA using fluorescence property form the PDI assemblies. (B) chemical structure for the **PDI-37** molecule and its working principle for the ATP detection based on turn-on fluorescence. (C-D) represents the chemical structure for **PDI-38** and a schematic diagram for the detection of Cu^{2+}, and PPi depending on the off-on fluorescence from **PDI-38.** (E-F) chemical structure for **PDI-39** and **40** for the detection of Con A. (G) changes in fluorescence spectra of **PDI-39** with ConA. (H) Changes in CD spectrum for **PDI-40** with added conA [84,98–100].

PDI-cored glycodendrimers **39** and **40** exhibited selective affinity towards Concanavalin A (Con A), attributed to the carbohydrate–lectin interactions between the mannose units on the glycodendrimers and Con A, which serves as a model lectin (Figure 8E,F) [99,100]. To analyze the binding mechanism, fluorescence spectroscopy and circular dichroism (CD) measurements were

 doi:10.20944/preprints202503.0667.v1

conducted. As illustrated in Figure 8G, increasing the concentration of Con A resulted in a gradual reduction in the fluorescence emission of **PDI-39**. This quenching effect occurs as the PDI backbones penetrate the hydrophobic region of Con A, facilitated by hydrogen bonding and hydrophobic interactions. Similarly, the addition of **PDI-40** led to a decrease in the CD signal of Con A, which originates from its β-sheet-rich secondary structure, accompanied by a bathochromic shift (Figure 8H). The diminished CD signal suggests a loss of secondary structure due to cross-linked complex formation. The decline in both fluorescence emission and CD signal intensity confirmed the interactions between Con A and glycodendrimers **39** or **40**.

The versatility of PDIs extends beyond just fluorescence; their structures can be modified to introduce various chemical functionalities. The incorporation of PDIs into nanomaterials and hybrid sensor systems represents an exciting frontier in biosensing applications. The combination of PDIs with nanostructured materials can lead to improvements in sensitivity and selectivity. Hao et al fabricated an immunosensor using PDI nanowires self-assembled on sensitized In_2O_3@$MgIn_2S_4$ S-scheme heterojunction platform. This sensor combined with nanostructured electrodes showed enhanced electron transfer and more pronounced signal output when detecting biological targets such as CA15-3 [101]. A nanosilica functionalized PDI derivative was fabricated by Yadav et al. [102]. This material showed good sensing ability towards 4-nitrocatechol, Ru (+3), Cu (+2) with LODs of 4.34 nM, 0.56 nM, and 0.43 nM, respectively. The material showed a good biosensing capability towards brine shrimp having Cu (+2) and Ru (+3).

5.2. Bioimaging Applications

Water-soluble PDIs have emerged as promising fluorophores for imaging applications due to their strong fluorescence and the ability to operate in the near-infrared (NIR) region. This property enhances tissue penetration and minimizes autofluorescence, making them suitable for in vivo imaging studies. The development of PDI-based nanoprobes capable of generating fluorescence in response to specific biological signals has opened new avenues for real-time cellular imaging.

5.2.1. PDI Molecules

Recent research has highlighted the use of PDI derivatives in cell imaging, where their intrinsic fluorescence allows for effective visualization of cellular structures and processes [5,6,78]. Zimmerman's group reported a polyglycerol-dendronized **PDI-41** with a single biotin for targeted fluorescence bioimaging (Figure 9A)[80]. When immobilized on a PEG-passivated surface via biotin–neutravidin linkages, **PDI-41** exhibited strong fluorescence, confirming its specificity. In living E. coli cells expressing biotinylated receptors, pre-incubation with streptavidin led to bright fluorescent spots on the cell surface, sometimes forming a helical pattern consistent with protein arrangement. These findings highlight **PDI-41**'s potential as a precise bioimaging label and suggest a novel biolabeling strategy using a fluorescent core linked to a multivalent periphery for targeting and therapeutic applications (Figure 9B). A guanidinium-dendronized **PDI-42** was used for imaging HeLa cell cytoplasm, showing efficient uptake and accumulation (Figure 9C,D) [103]. Fluorescent positively charged dendritic star polymers (**PDI-43**, **PDI-44**, and **PDI-45**, Figure 9E) successfully entered living cells, while negatively charged counterparts (**PDI-8** and **PDI-9**) with carboxylic acids did not. Confocal microscopy confirmed the cell penetration of **PDI-43a** as shown in Figure 9F [104]. The study found that PDIs with a higher polymer chain density and fewer amino groups entered cells more rapidly, whereas those with more amino groups exhibited significant cytotoxicity.

 doi:10.20944/preprints202503.0667.v1

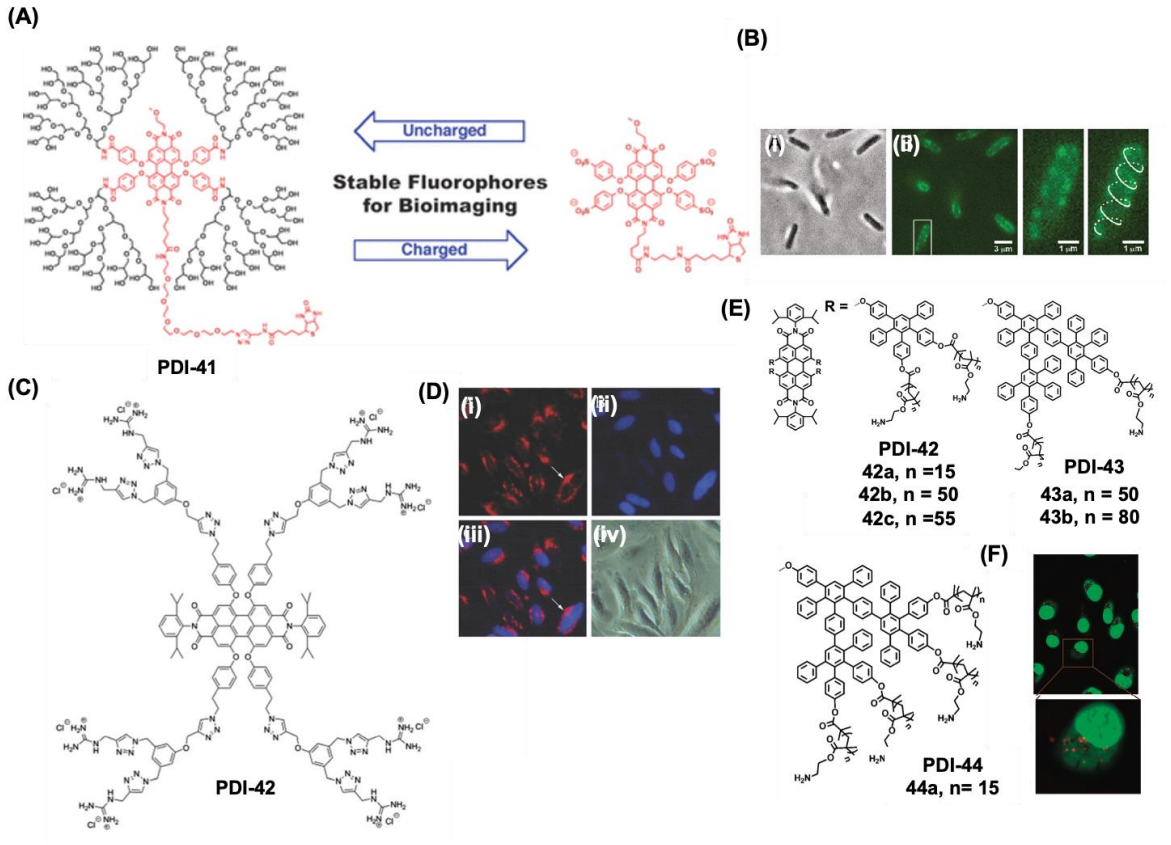

Figure 9. Chemical structures of **PDI-41-44** for bioimaging applications. (A) Chemical structure and (B) Bright-field and fluorescence images of E. coli labeled with **PDI-41**. (C) Chemical structure and (D) Fluorescence microscopy images of HeLa cells incubated with **PDI-42** for 24 h, showing red fluorescence in the cytoplasm (i) and DAPI-stained nuclei (ii). Merged (iii) and brightfield (iv) images highlight ongoing cell division. (E) Chemical structures of PDI-42-44 and (F) **PDI-43a** (red) penetrating ECV-304 cells stained with a green fluorescence tracker. [80,103,104].

An amphiphilic PG-dendronized **PDI-45** was developed as a membrane marker, incorporating two alkyl chains to anchor within lipid bilayers (Figure 10A)[105]. In water, **PDI-45** formed micellar aggregates and remained nearly nonfluorescent. However, upon integration into biological membranes, the micelles disassembled, restoring the fluorescence of the perylene core (Figure 10B). Cellular studies showed **PDI-45** localized in the plasma membrane and Golgi, suggesting uptake via endocytosis. Its passive diffusion was confirmed by a lack of colocalization with BODIPY TR methyl ester, except in the Golgi (Figure 10C). This makes PG-dendronized **PDI-45** a valuable tool for tracking PG-bound bioactive compounds in membranes.

A new series of highly fluorescent and water-soluble tetrapodal PDI dye termed PDI-4Py-n, (**PDI-46**) has been synthesized by Cui et al. (Figure 10D)[106]. These dyes consist of a central chromophore core surrounded by four pyridinium groups, which create spatial separation and electrostatic repulsion, effectively minimizing chromophore aggregation even in relatively concentrated aqueous environments. As a result, **PDI-46** maintains strong fluorescence with a high photoluminescence quantum yield. Due to their exceptional fluorescence characteristics and biocompatibility, one of these dyes has been successfully employed as a lysosome-specific fluorescent probe for live-cell imaging (Figure 10E**)**. This work presents a straightforward synthetic strategy for producing water-soluble, non-aggregating organic dyes and highlights their significant potential in biomedical applications. Yang et al. reported an azetidine substituted PDI derivative with a multicolor cell imaging capability (**PDI-47**) (Figure 10F)[107]. Fine tuning the electron electron donating capability of the azetidine at the bay positions a shift in NIR fluorescence with a Stokes shifts increasing from 35 to 110 nm with a shift in color from visible to red region. The fabricated dyes

 doi:10.20944/preprints202503.0667.v1

showed good cell-permeability and they selectively stained various organelles for multicolor imaging of multiple organelles in living cells (Figure 10F). Moreover, the carboxylic acid terminated PDI derivative showed in vivo imaging capability for tumor bearing mice (Figure 10F). A water-soluble PDI-cyclophane has been developed by incorporating a central PDI chromophore enclosed by two cationic molecular straps (**PDI-48**) (Figure 10G)[108]. This design effectively prevents chromophore self-aggregation in aqueous environments by ensuring spatial separation. Consequently, the cyclophane is highly suitable for lysosome-specific live-cell imaging and possess excellent photothermal effect with antibacterial properties (Figure 10H).

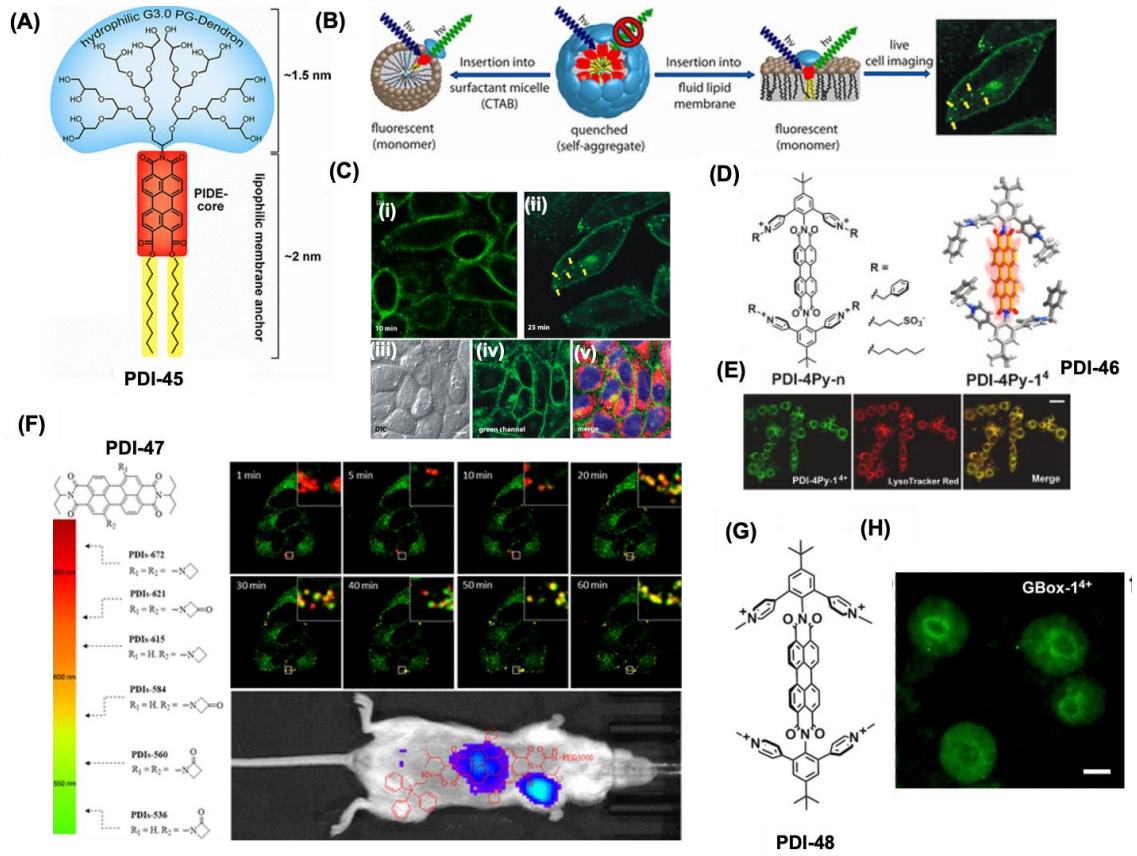

Figure 10. (A) Chemical structure of amphiphilic perylene dye **PDI-45** for biological membrane imaging. (B) Schematic of self-quenching and monomerization in different environments for **PDI-45** dye. (C) Confocal images of CHO cells incubated with **PDI-45**: (i) 10 min incubation labels the plasma membrane, (ii) 25 min incubation shows endocytic uptake, with vesicles (yellow arrows) likely trafficking to the Golgi. (iii–v) Costaining with BODIPY-TR (red) for intracellular membranes and DAPI (blue) for nuclei shows colocalization at the Golgi (yellow). (D-E) **PDI-46** structure and fluorescence colocalization with Lyso Tracker Red in RAW 264.7 cells (scale: 25 μm). (F) **PDI-47** structure with tunable NIR emission via azetidine substitutions, confocal imaging in HeLa cells and in vivo tumor imaging. (G-H) **PDI-48** structure and RAW 264.7 cell imaging application (scale: 5 μm) [105–108].

N-Cyclic bay-substituted **PDIs** have been identified as G-quadruplex ligands capable of inducing DNA damage in cancerous cells [109]. Alterations in the terminal groups or variations in the side chain length at the imide positions had minimal impact on their binding affinity to the G-quadruplex structure of the human telomeric sequence. However, modifications in the bay-region, including the type and number of substituents, significantly influenced their interaction. When transformed human fibroblasts were treated with this **PDI**, deconvolution microscopy revealed that certain damaged sites containing phosphorylated 53BP1, a key DNA damage response protein, co-localized with TRF1, a marker for interphase telomeres. This led to the formation of telomere-dysfunction induced foci. These findings suggest that the G-quadruplex targeting **PDI** functions as a telomere inhibitor, highlighting its potential as a selective anticancer agent.

 doi:10.20944/preprints202503.0667.v1

5.2.2. PDI Based Nanoparticles

PDI nanoparticles (**PDI-NPs**) have been increasingly recognized for their utility in various bioimaging modalities. For instance, NIR fluorescence imaging capitalizes on the thermal stability of PDIs, enabling efficient imaging with minimal background interference. The development of NIR-II fluorescence imaging agents using PDIs has paved the way for deeper tissue penetration, thus achieving high-resolution imaging with significant practical applications in diagnosing and monitoring cancer therapies.

Zong et al. prepared **PDI-49 NPs** with 1,3-di(9H-carbazol-9-yl) benzene as an isolation group for controlling the aggregation of parent PDI derivative (**PDI-49)** (Figure 11A)[86]. The PDI NPs were prepared by nanoprecipitation method using the emulsion matrix as Pluronic F-127 (F127) as shown in Figure 11B. These **PDI-NPs** showed excelled photostability and retained their fluorescence intensity up to 79% after irradiating using a continuous laser excitation (450 nm, 100 mW) for 3 h (Figure 11C). The morphology of these **PDI-49 NPs** was analyzed using transmission electron microscopy (TEM), while their average hydrodynamic diameter was determined to be approximately 100 nm through dynamic light scattering (DLS) (Figure 11D). In an aqueous medium, **PDI-49**-exhibited a bright deep-red emission with a maximum wavelength at 658 nm and a quantum yield (Φ) of 2.37%, as observed from the single-photon fluorescence spectrum. Utilizing three-photon excited fluorescence microscopy technology, **PDI-49 NPs** enable skull imaging of the mouse cerebral vasculature (Figure 11E). This approach achieves a remarkable penetration depth of up to 450 μm.

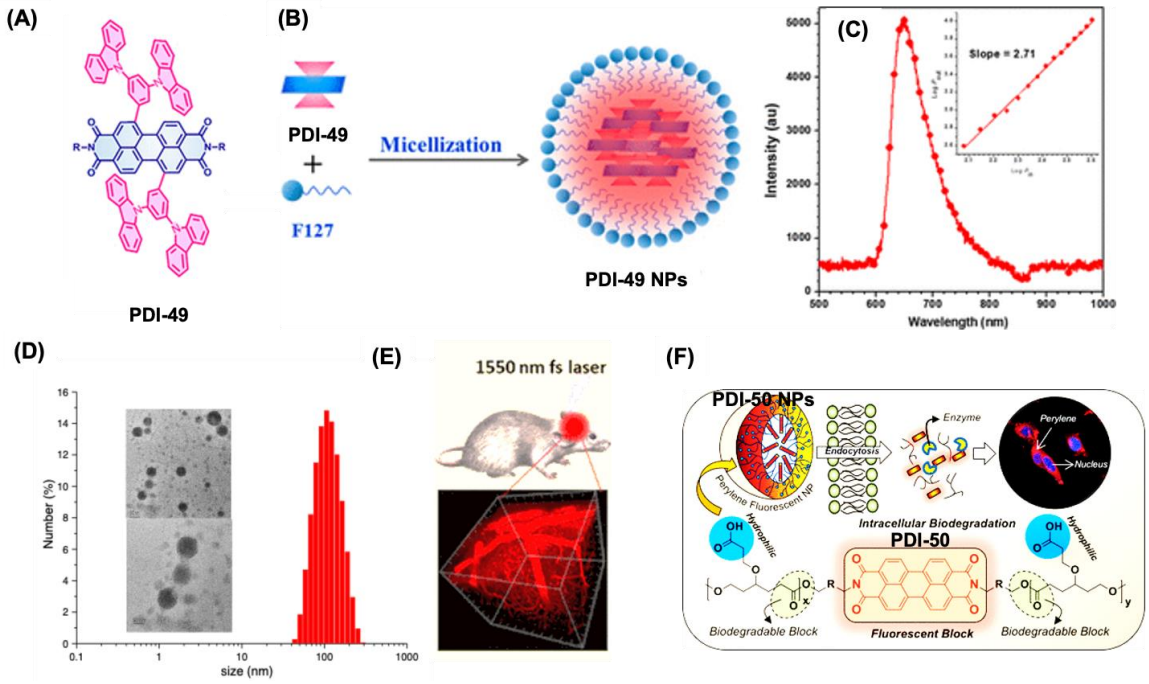

Figure 11. Various PDI-NPs for bioimaging applications. (A) Chemical structure of PDI-49, and (B) formation of **PDI-49 NPs** from **PDI-49** after micelle formation using F127. (C) Emission spectra for the **PDI-49 NPs** after laser exposure. (D) represets the TEM and DLS profiles for **PDI-49 NPs**. (E) A reconstructed 3D image showing the distribution of the **PDI-49 NPs** in blood vessels of the mouse. The scale bar: 100 μm. (F) A schematic for the design and development of PDI-tagged amphiphilic PCL block copolymers and their nanoassembly formation (**PDI-50 NPs**) and intracellular enzyme-responsive bio-imaging application [86,110].

A biodegradable and enzyme-responsive red fluorescent polycaprolactone (PCL) block copolymer, tagged with **PDI-50** was developed as a nanoprobe (**PDI-50 NPs**)for intracellular imaging in both normal and cancerous cells (Figure 11F) [110]. The synthesis involved the symmetrical bis-imidization of PTCDA, yielding a bis-hydroxyl functionalized PDI derivative, which then served as an initiator for ring-opening polymerization, achieving up to 40 repeating units. The removal of tert-

 doi:10.20944/preprints202503.0667.v1

butyl ester groups led to the formation of amphiphilic PDI-CPCLx block copolymers. Due to the self-assembly of the carboxyl-containing segments, these copolymers formed nanofibrous structures in organic solvents and stable spherical nanoparticles (**PDI-50 NPs**) of approximately 100 nm in aqueous media. Additionally, the NPs exhibited a quantum yield (Φ = 0.25–0.30), making them highly suitable for bioimaging. Cytotoxicity assessments demonstrated excellent biocompatibility, with the **PDI-50 NPs** accumulating around the perinuclear region of both normal and cancer cells, following cellular uptake via the endocytosis pathway (Figure 11F).

A novel amphiphilic diblock copolymer, was synthesized via RAFT polymerization to address the limited NIR emission of water-soluble PDI-based probes [111]. This copolymer exhibited enhanced π–π stacking compared to the PDImonomer, leading to a red-shifted emission at 620 nm in chloroform. In aqueous solution, stronger π–π interactions promoted self-assembly into uniform polymer nanoparticles with an average size of ~65 nm. These nanoparticles demonstrated efficient cytoplasmic localization in human pancreatic cancer cells, highlighting their potential for NIR-based bioimaging applications. An asymmetric PDI derivative with a hydrophobic tail and a hydrophilic zwitterionic head was synthesized using a stepwise amine addition, yielding 12% [112]. It exhibited fluorescence at 542 nm with a shoulder at 584 nm, reducing autofluorescence in bioimaging. Due to π–π stacking, it self-assembled into nanosized vesicles in water (Φ = 0.1) but remained dispersed in DMSO (Φ = 0.67). These vesicles interacted with cell membranes via electrostatic attraction and disassembled in the presence of DPPC micelles, enabling intracellular membrane labeling through hydrophobic interactions.

A water-soluble silicon quantum dots-N-propylurea-PDI assembly was prepared by Abdelhameed et al. [113]. This quantum dots effectively enabled the fluorescent imaging in HEK293 and U2OS cells. These 1.6 nm nanoparticles were synthesized by heating PTCDA with 3-aminopropyl) triethoxysilane, pre-reduced using trisodium citrate dihydrate in glycerol. The Urea-soluble silicon quantum dots -PDI exhibited pH sensitivity, with reduced emission at 480 nm in the pH range of 2.6–4. Intramolecular hydrogen bonding between the amine hydrogen and diimide oxygen likely hindered electron transfer, suggesting energy transfer as the primary cause of emission quenching.

Ribeiro et al. report the synthesis of highly bright and photostable fluorescent silica nanoparticles (SiNPs) with emission in the visible and NIR range [114]. These nanoparticles, ranging from 30 to 300 nm in diameter with low size dispersity, incorporate alkoxysilane-modified PDI dyes that integrate into the silica structure. The green-emitting (PDI) and NIR-emitting (PDInir) dyes exhibit fluorescence quantum yields of 90% and 24%, respectively. HEK293 cells efficiently internalized these SiNPs with minimal toxicity, demonstrating exceptional photostability. The NIR-emitting nanoparticles are particularly suited for multi-color imaging, even in cells with high fluorescent protein expression or co-stained with common fluorophores emitting at lower wavelengths.

5.2.3. Photoacoustic Based Imaging (PAI)

The intrinsic properties of PDIs significantly enhance their efficacy as photoacoustic agents (PA). The substantial absorption coefficients and fluorescence quantum yields of PDIs allow for effective conversion of absorbed light energy into ultrasound signals, making them suitable for high-resolution imaging of deep tissues. Recent developments have demonstrated that PDI-based nanoparticles can serve as highly efficient photoacoustic contrasting agents.

Fan et al. designed a PDI derivative with tertiary amine group as electron withdrawing and diimdie as electron acceptor group for fabricating a NIR absorbing derivative (**PDI-51)** (Figure 12A) [115]. To improve the water solubility DSPE-mPEG-5000 was used as surfactant to form **PDI NPs** with an average size of 48 nm. These NPs showed an NIR absorption of 700 nm, with a molar extinction coefficient of $2x10^8$ M^{-1} cm^{-1}. The as prepared **PDI NPs** showed excellent photostability, serum stabilities as compared with commercial ICG dye for photoacoustic applications. These **PDI NPs** were successfully used to realize a PAI of deep orthotopic brain tumours in mouse models, showing that they could act as PA contrast agent for in vivo deep-brain tumors with a simple detection using the EPR effect. PA spectra confirmed **PDI NP** localization in brain tumors. Figure 12B

 doi:10.20944/preprints202503.0667.v1

shows strong PA signals at 700 and 735 nm (blue line) two days post-injection, matching the NIR absorption peak of PDI NPs and their PA peaks in solution (black line). This differs from pre-injection signals (red line), indicating successful tumor accumulation (Figure 12C). The 3D ultrasound (US) and PA imaging effectively mapped the spatial distribution of PDI NPs in the tumor. The NPs localized near the C6-Fluc cell injection site, demonstrating their high-quality 3D PAI capability for tumor imaging.

A recent study provided the first evidence of using PDI NPs for tracking mesenchymal stromal cells (MSCs) (Figure 12D). The key to stabilizing these nanoparticles was the incorporation of a star-shaped hyperbranched polymer (SHBP) within the PDI-NPs (**PDI-52 NPs**). Even 11 days after injecting MSCs labeled with **PDI -52 NPs**, a strong PA signal was still detectable, confirming their persistence within the cells (Figure 12E). Notably, the study ruled out false positives, demonstrating that PDI NPs were not phagocytosed by macrophages following the apoptosis of labeled MSCs. This suggests their suitability for long-term cell tracking.

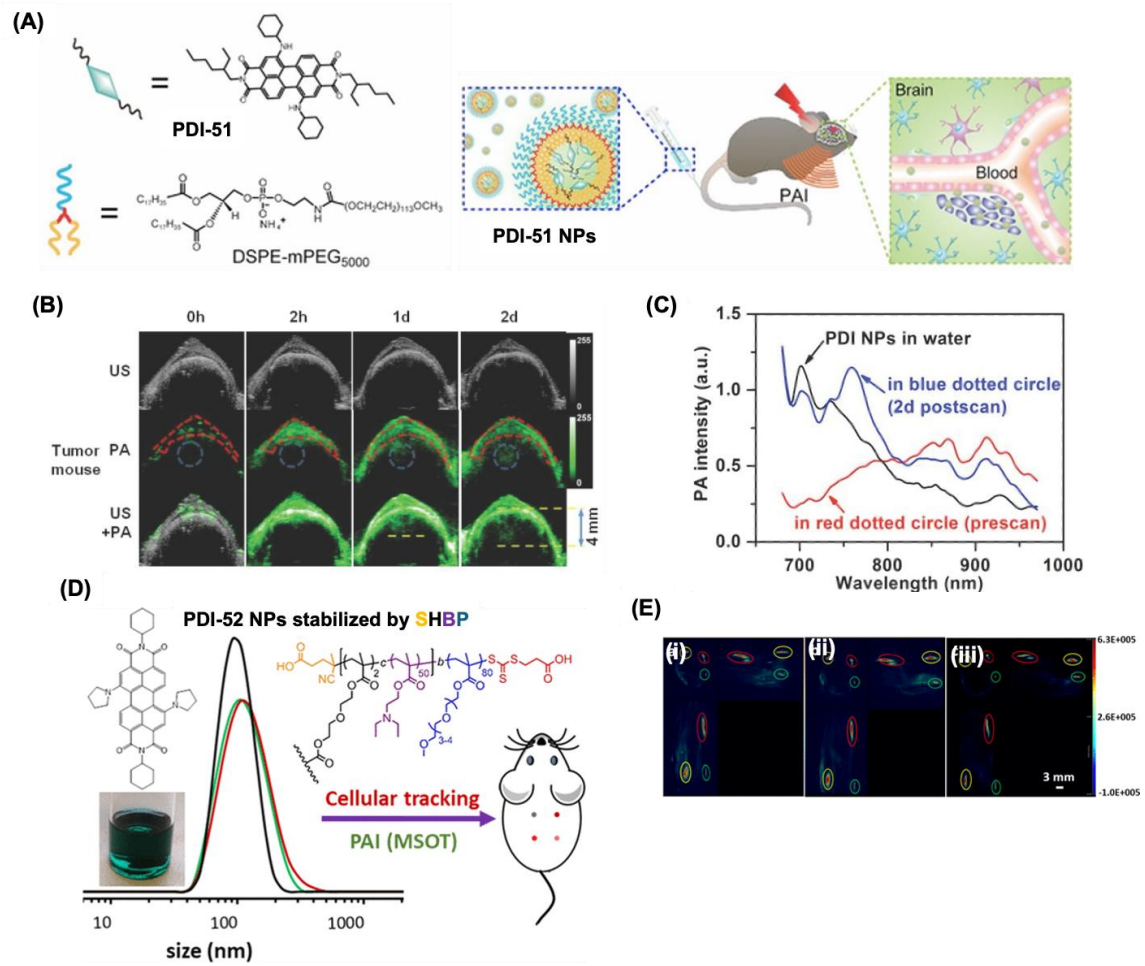

Figure 12. PDI based NPs for photoacoustic imaging. (A) Chemical structure and application of **PDI-51 NPs** for PAI application. (B) The US (grey), PA (green), and their overlay coronal sections of brain tumor model (bottom) before and after tail vein injection of 250 μL of 250 nM **PDI-51NPs**. (C) PA spectra of **PDI-51 NPs** in aqueous solution (black line), the region in red dotted circle of (B) before injection of NPs (red line) and tumor region of (B) after 2 d injection of NPs (blue line). (D) Chemical structure for **PDI-52**, and formulation for **PDI-52 NPs**. (E) MSOT 3D images of a mouse injected with MSCs on days 1 (i), 7 (ii) , and 11 (iii), showing transverse, sagittal, and coronal views. Red, yellow, and green circles indicate 1×10^6, 0.5×10^6, and 0.25×10^6 **PDI-52 NPs** labeled cells, respectively. Cell locations are determined by PDI signal intensity after spectral unmixing, with consistent length and color scales across images [115,116].

 doi:10.20944/preprints202503.0667.v1

Cui et al. modified cRGD on the PEG surface of PDI NPs to create cRGD-PDI NPs, which targeted early thrombus via GPIIb/IIIa [117]. In a mouse thrombus model, these NPs were injected and exposed to a 700 nm NIR laser for PAI. The PA signal of early thrombus was four times higher than that of older thrombus, allowing clear differentiation. Comparative imaging studies showed that US and MRI were ineffective in detecting thrombus formation, whereas PAI provided high spatial contrast, revealing vessel morphology and early thrombus. After urokinase injection, the PA signal decreased to normal levels. The study also found that PA intensity correlated with NP size and concentration, highlighting the need to optimize these factors for effective PAI.

5.3. PDI NPs for Cellular pH Measurements

PDI-NPs utilize a pH-sensitive fluorescence response mechanism to monitor the local pH environment within cells. The fluorescence intensity of PDI is highly dependent on the local pH, where specific changes in pH lead to alterations in the electronic state of the PDI molecule, affecting its fluorescence emission. For instance, PDI molecules can exhibit a remarkable fluorescence increase in acidic conditions due to the protonation of specific functional groups, which enhances the fluorescence quantum yield. This pH-dependent fluorescence response is particularly advantageous for monitoring pH variations in cellular compartments, aiding in the understanding of cellular processes such as metabolism, apoptosis, and disease progression [118,119]. Ma et al. developed a water-soluble pH probe (**PDI-53**), by introducing four carboxyl lipid chains into the perylene core for intracellular pH detection in A549 cells and E. coli (Figure 13A) [120]. The addition of an O− group enhanced pH sensitivity through protonation and deprotonation. As pH increased, **PDI-53** deprotonated to **PDI-53**−, leading to a high negative electrostatic potential in the aromatic nucleus, which weakened fluorescence intensity. The probe exhibited a strong fluorescence response with a linear relationship in the pH range of 6.9–8.9, enabling quantitative pH measurement. When co-incubated with E. coli and A549 cells, fluorescence intensity decreased with rising extracellular pH, becoming nearly quenched at pH 8.9 (Figure 13B). These findings highlight HPTBAC as a promising tool for pH monitoring in living cells.

A reversible fluorescence pH probe, **PDI-54,** was recently developed for detecting strong acidic conditions by Ye et al. (Figure 13C) [121]. Based on the PET mechanism, its fluorescence intensity significantly increased as pH dropped from 4.0 to 2.6 under 555 nm laser irradiation (Figure 13D). Additionally, Georgiev et al. found that the internalization of a perylene diimide probe (**PDI-55**) in L929 cells was concentration dependent [93]. At 1.3 μM, the probe successfully penetrated cells, but at concentrations above 26 μM, internalization was inhibited, likely due to the formation of micro-sized aggregates [Figure 13E).

 doi:10.20944/preprints202503.0667.v1

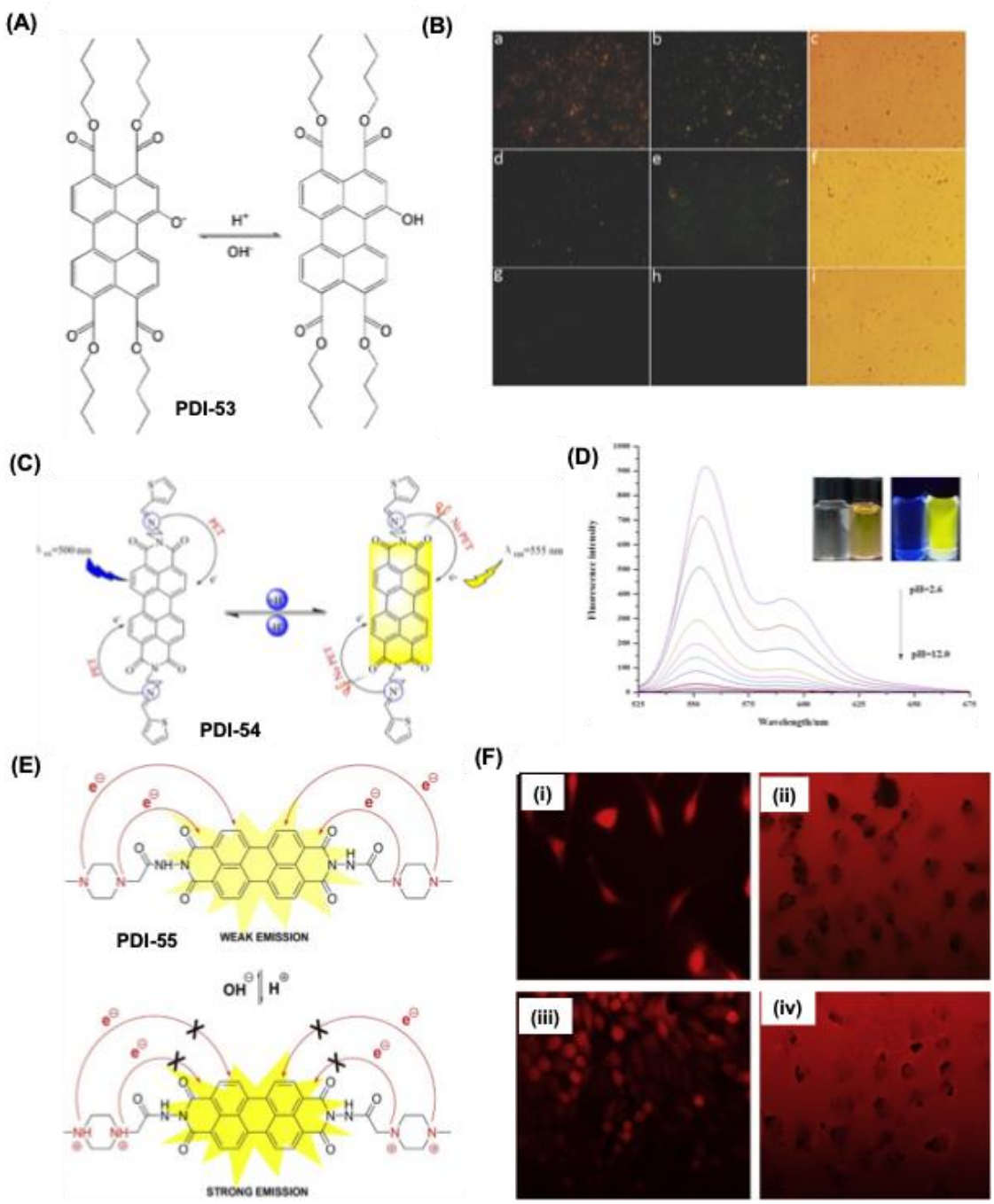

Figure 13. PDI based pH sensors. (A) Chemical structure of **PDI-53** and its pH-responsive switching mechanism. (B) Fluorescence imaging of E. coli stained with 50 mM **PDI-53** for 1 hour at pH 6.7 (a–c), 8.0 (d–f), and 8.9 (g–i). Images captured in the blue channel (460–490 nm) (a, d, g), green channel (530–590 nm) (b, e, h), and bright field (c, f, i). (C) Proposed pH-sensing mechanism of **PDI-54.** (D) Fluorescence spectral variations of **PDI-54** at different pH levels, with inset showing color changes under UV light. (E) Chemical structure and pH response mechanism of P**DI-55**. (F) Microscopic visualization of **PDI-55** micelles in living L929 cells after 24 h (top) and 48 h (bottom) incubation at 1.3 μM (i, iii) and 26 μM (ii, iv). Scale bar: 50 μm [93,120,121].

5.4. PDI for Drug Delivery and Cancer Therapy

PDI derivatives exhibits strong self-assembly behavior due to π–π interactions between its perylene cores, enhancing NIR absorption and power conversion efficiency with a red-shifted absorption. Researchers have explored self-assembled PDI-based nanodrugs for tumor therapy, valued for their simplicity, eco-friendliness, high drug-loading capacity, and low toxicity. A common approach involves modifying the imide- and bay-regions with hydrophilic functional groups like

 doi:10.20944/preprints202503.0667.v1

polymers and photosensitizers to create amphiphilic derivatives [90,122–124]. These derivatives self-assemble into multifunctional nanocarriers through π–π stacking, hydrogen bonding, and hydrophobic interactions. At the tumor site, controlled drug release enhances local drug concentration, minimizes systemic toxicity, and enables fluorescence imaging-guided chemotherapy, photothermal, and photodynamic therapy, resulting in significant tumor inhibition.

Yang et al. developed two asymmetric amphiphilic PDI derivatives **PDI-56, PDI-57** and created self-assembled **PDI-58 NPs** of sizes 30, 60, 100, and 200 nm by adjusting the initial PDI concentration (Figure 14A) [125]. These NPs were used as PA probes and photothermal agents, with size-dependent aggregation observed in tumors through PA and PET imaging using [^{64}Cu]-labeling. The study found that 60 nm **PDI NPs** provided the best tumor imaging and treatment efficacy, showing the highest tumor accumulation (Figure 14B,C). Under 675 nm irradiation, the tumor temperature rose with prolonged exposure (Figure 14D), and after 10 days, the tumor was fully eliminated.

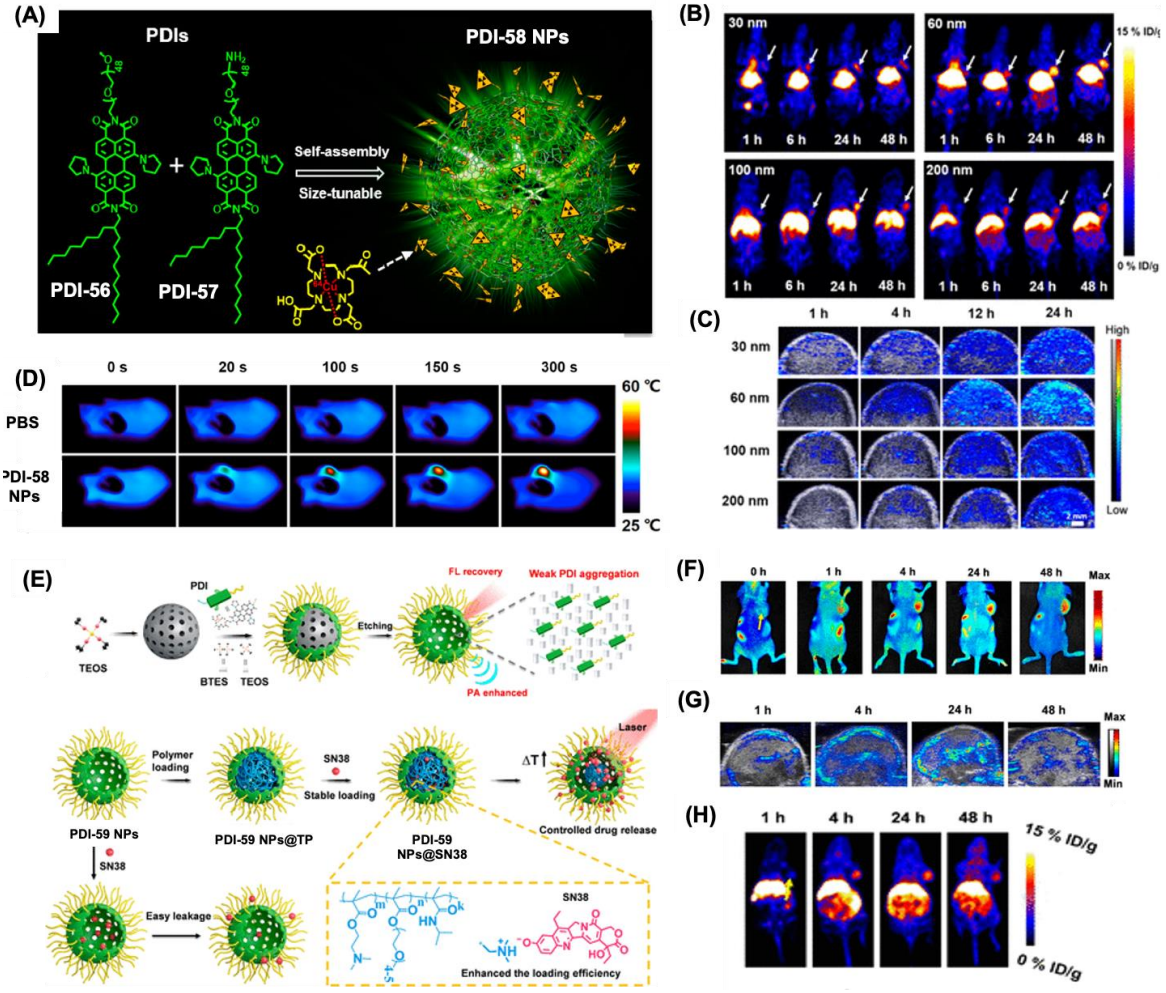

Figure 14. Theragnostic application of PDI derivatives. (A) Design scheme for **PDI-58 NPs** using self-assembly method. (B) Decay-corrected coronal PET images of small animals captured at 1, 6, 24, and 48 hours post-intravenous injection of **PDI-58 NPs** of varying sizes, with white arrows indicating U87MG tumors. (C) Merged coronal PA and US images of U87MG tumors obtained at 1-, 4-, 12-, and 24-hours following injection of different sized **PDI-58 NPs**. (D) Infrared thermal images of U87MG tumor-bearing mice under 675 nm laser irradiation (1 W/cm^2) at 24 hours post-injection of PBS or **PDI-58 NPs.** (E) Development and fabrication of **PDI-59**@TP-SN38 for multimodal imaging-assisted, light-triggered combined photothermal and chemotherapy. (F) In vivo FL images and (G) PA images of U87MG tumor-bearing mice at various time points postinjection of **PDI-59 NP**s. (H) PET imaging for the whole-body tracking of ^{64}Cu-labeled **PDI-59 NPs** (arrow points at the tumor site) [125,126].

 doi:10.20944/preprints202503.0667.v1

Yang et al. developed a photo-responsive cancer theranostic platform, HMPDI@TP-SN38 (**PDI-59 NPs**), using an "in situ skeleton growth" method for precise, on-demand PTT/Chem therapy guided by FL/PA/PET imaging [126]. **PDI-59 NPS@SN38** were synthesized via co-hydrolysis of PEG2000–PDI–silane and silica precursors. Ammonia etching selectively removed the mesoporous silica core, forming a hollow PDI shell which was then grafted with thermosensitive polymers. This structure enhanced FL/PA signals and improved drug tracking. Upon near-infrared irradiation, PDI generated heat, contracting thermosensitive polymer and releasing SN38, minimizing drug leakage while increasing loading efficiency. Nanotheranostics integrates diagnosis and therapy into a single system, enabling real-time tracking of drug distribution and targeted treatment for personalized medicine [127]. In 2018, Chen et al. developed, a pH-sensitive nano-thermosensitive agent using PDI derivatives modified with N-methylpiperazine and PEG2000 (**PDI-60 NPs**) (Figure 15A) [128]. This system, incorporating IR825 dye as an internal reference and doxorubicin (DOX), self-assembles under neutral conditions via hydrophobic and π–π interactions. In the acidic tumor microenvironment, protonation enhances hydrophilicity, deforming NPs at pH 5.5 and triggering DOX release (Figure 15B). The ratiometric PAI using IR825 dye precisely monitors pH-responsive drug release, optimizing chemotherapy and tumor suppression (Figure 15C,D).

An asymmetric theranostic nanoparticle (PDI–IR790s–Fe/Pt) was designed to enhance ROS generation and enable real-time monitoring of chemotherapy via ratiometric PA imaging [129]. Self-assembled from a PDI-based cisplatin prodrug, IR790s, and chelated ferric ions, its structure was directed by polyphenol–iron coordination, while a PEG chain improved water solubility. The prodrug released cisplatin in the tumor microenvironment, triggering oxygen conversion to superoxide radicals and H_2O_2 formation. Strong NIR absorption at 680 nm enabled PA imaging, allowing real-time tracking of ROS production and therapeutic response at excitation wavelengths of 680 and 790 nm.

Ultrasound imaging (USI) is widely used in clinics due to its noninvasiveness, lack of ionizing radiation, and affordability. Combining USI with PA imaging enhances spatial resolution and deep-tissue penetration. Recently, phase-changeable perfluorocarbon nanodroplets have emerged as promising ultrasound contrast agents due to their superior tumor vascular permeability. A photoacoustic nanodroplet, PS-PDI-PAnD, was developed to stabilize low-boiling-point perfluorocarbon droplets, utilizing PDI-PEG-OMe as a photoabsorber and ZnF16Pc as a photosensitizer [130]. Designed for amphiphilicity, the PDI shell stabilizes the nanodroplets through strong π–π interactions. Upon 671 nm laser irradiation, the PDI shell converts light into heat, inducing perfluorocarbon phase transition for enhanced USI and a photothermal effect. Simultaneously, ZnF16Pc generates cytotoxic singlet oxygen ($^1O_2$), boosting the PDT effect.

A semiconducting-plasmonic nanovesicle, Au@PPDI/PEG, was developed through the self-assembly of semiconducting poly(PDI) (PPDI) and PEG-tethered gold nanoparticles [123]. This nonconjugated polymer with pendant PDI units was synthesized via post-polymerization modification. The precursor copolymer, made from styrene and poly(pentafluorophenyl acrylate) was prepared using ATRP with DTBE as an initiator. Gold nanoparticles (AuNPs) were introduced via disulfide functionality, forming covalent Au-S bonds on their surface. Featuring strong NIR absorption, the plasmonic coupling of AuNPs enhanced light absorption and PA signal of PPDI. In vivo studies confirmed its potential as a high-resolution tumor imaging probe with improved photothermal efficiency for cancer theranostics. A supramolecular drug delivery system was developed using two oppositely charged components: a fluorescent star polycation (**PDI-61**) conjugated to camptothecin via a reduction-responsive bond and an anionic copolymer (P2) (Figure 15E) [131]. Their interaction formed a stable complex (**PDI-61@P2**) that accumulated at tumor sites via the EPR effect. In the acidic tumor microenvironment, bond cleavage triggered charge conversion and complex disassembly, enhancing cellular uptake. The “proton sponge” effect facilitated prodrug release, followed by disulfide-bond cleavage in response to glutathione (GSH), ultimately releasing the drug camptothecin into the nucleus to induce cancer cell apoptosis (Figure 15F). This system

Preprints.org (www.preprints.org) | NOT PEER-REVIEWED | Posted: 10 March 2025 doi:10.20944/preprints202503.0667.v1

exhibited superior tumor inhibition compared to free camptothecin, highlighting its therapeutic potential (Figure 15G).

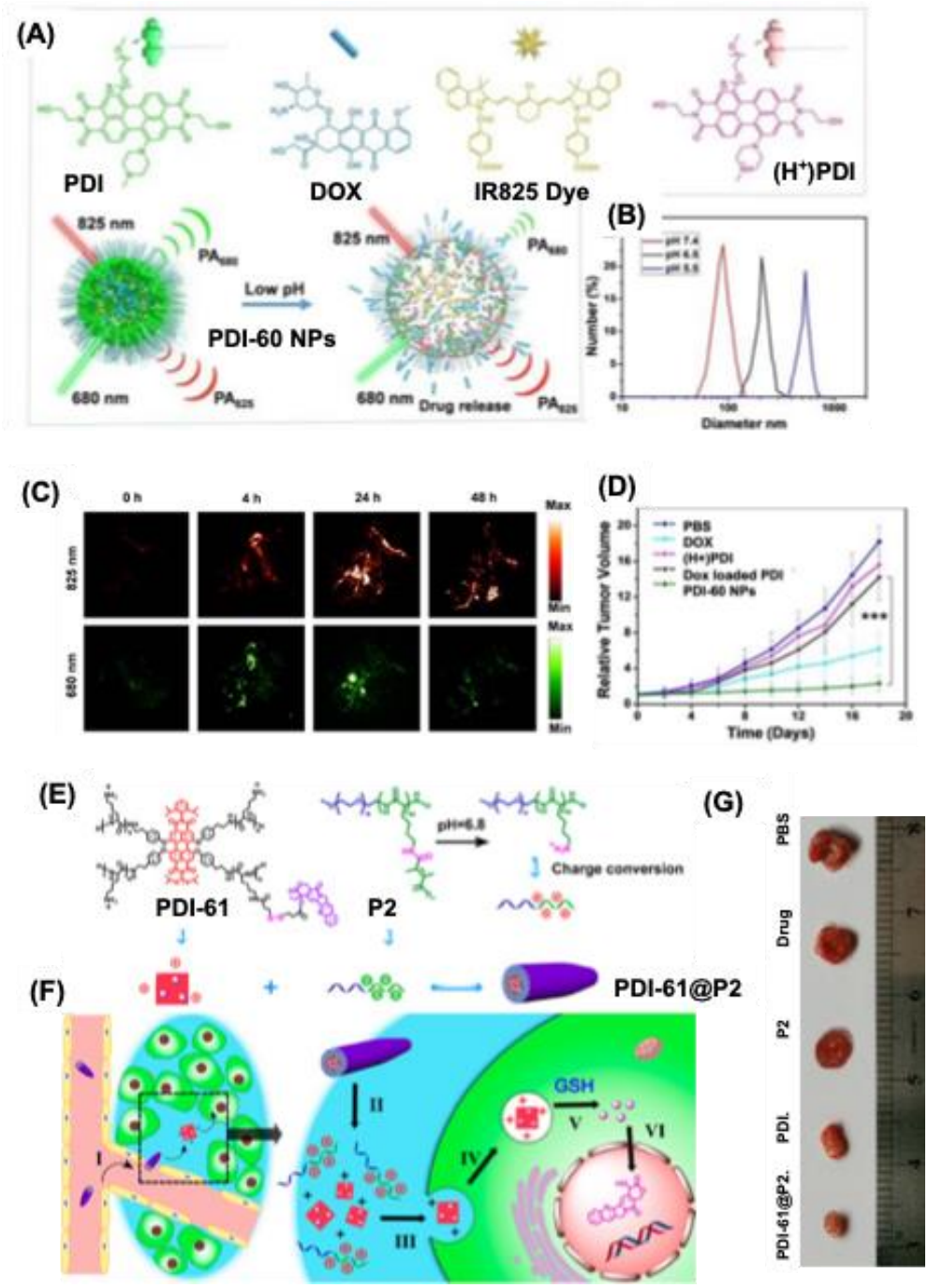

Figure 15. PDI derivatives for cancer treatment. (A) A schematic representation for the formation of PDI-60 NPs and their mechanism for DOX release with pH changes. (B) change in the size of PDI-60 NPs with varying pH conditions. (C) In vivo photoacoustic images for a subcutaneous U87MG tumor in a nude mouse after intravenous administration of the PDI-60 NPs at various time intervals. (D) Tumor growth in the U87MG tumor mice with PDI-60 NPs with various controls. ***, $P < 0.001$. (E-F) Formation of PDI-61@P2 assembly and the mechanism of release for camptothecin with GSH. (G) Photographs of tumors after different treatments on the 12th day [128,131].

Li et al. developed triphenylamine-perylene diimide conjugate-based nanoparticles for photoacoustic imaging and cancer phototherapy [132]. The NPs were prepared via nanoprecipitation and the NPs exhibited good water dispersibility with an average size of ~70 nm with a strong NIR

 doi:10.20944/preprints202503.0667.v1

absorption. The NPs showed a high photothermal conversion efficiency up to 46.1%. Under 635 nm laser irradiation, they generated strong photoacoustic signals and induced reactive oxygen species in aqueous solutions and cancer cells. MTT assays confirmed their biocompatibility and potent photocytotoxicity, making these NPs a promising for photoacoustic imaging and photothermal/photodynamic therapy.

Using the mixed imide–anhydride intermediate, a luminescent rhenium(I)–polypyridine complexes conjugated with PDI moiety was fabricated recently [133]. The PDI moiety is attached to the rhenium complex via a disulfide bond. This linker prevents direct electronic interaction while enabling thiol-sensitive redox activity for drug delivery. The interaction between the metal complex and fluorescent units facilitates FRET and find applications in bioimaging, sensing, and photocytotoxicity. Notably, the complex showed high singlet oxygen generation under 365 nm irradiation, effectively killing HeLa cancer cells, highlighting its potential as a photodynamic therapeutic agent.

Synergistic photodynamic therapy and photothermal therapy can enhance treatment efficacy; however, conventional PDT/PTT agents require activation at two different laser wavelengths, complicating the process and extending treatment time [134,135]. To address this, in 2018, Fan et al. developed a novel photosensitizer (PDS-PDI), from 2-(Dimethylamino) ethyl methacrylate and PDI, through atom transfer radical polymerization [136]. This amphiphilic polymer, modified with sulfonic acid, exhibited high photothermal conversion and efficient singlet oxygen generation (16.7%) under a single 660 nm wavelength, making it suitable for combined PDT/PTT therapy. Injectable hydrogels are a promising localized drug delivery system due to their minimally invasive application and precise drug release at tumor sites, reducing systemic toxicity. In a subsequent study, the same research team introduced a dynamic covalent hydrogel (GelPV-DOX-DBNP) containing PDS-PDI, ascorbic acid (Vc), the chemotherapy drug doxorubicin (DOX), and photothermal nanoparticles [137]. Upon 660 nm light exposure, singlet oxygen from PDS-PDI was converted into hydrogen peroxide by Vc, breaking the hydrogel's dynamic covalent bonds. Concurrently, the hydrogel transformed into a liquid with increasing temperature, accelerating the release of DOX and photothermal nanoparticles, demonstrating an effective PTT/chemotherapy combination approach.

Heavy-metal-based PDT materials enhance ISC by generating triplet excitons that facilitate ROS production via type I and/or type II processes [138]. However, their potential toxicity raises health concerns. In contrast, metal-free organic materials are more biocompatible but typically yield lower ROS levels. Recently, sulfur-containing compounds have gained attention due to their potential biocompatibility. Sulfur, being slightly heavier than oxygen, promotes ISC and triplet exciton formation via the n-π^* transition. Dithionated PDIs, specifically trans-isomer PDI-TS and cis-isomer PDI-CS, were synthesized using Lawesson's reagent, albeit with low yields of 5.5% and 10.9%, respectively [139]. These thiono-PDIs exhibit red-shifted absorption in the NIR region [140]. Nanoprecipitation produced PDI-CS and PDI-TS nanoparticles of approximately 55 nm, a size suitable for tumour targeting via the EPR effect. UV-Vis spectra revealed absorption peaks between 500–700 nm in THF, indicating a nonaggregated state. In water, PDI-TS NPs showed weak absorption around 560 nm with a new peak at 660 nm, suggesting π–π interactions. Upon 660 nm light irradiation, PDI-TS NPs exhibited strong photothermal effects in A549 cells, achieving a photothermal conversion efficiency of 58.4%, compared to 41.6% for PDI-CS NPs. Additionally, PDI-TS NPs generated ROS under laser exposure and demonstrated tumour growth inhibition, highlighting their potential for cancer therapy. This strategy was recently applied to thiono-PDI derivatives containing one to four sulfur atoms, including 1S-PDI-D, 2S-cis-PDI-D, 2S-trans-PDI-D, 3S-PDI-D, and 4S-PDI-D. Notably, increasing sulfur substitution shifted the maximum absorption into the NIR region while enhancing the molar extinction coefficient. These compounds are non-emissive in common organic solvents, likely due to rapid ISC quenching fluorescence. However, they exhibited strong two-photon absorption.

 doi:10.20944/preprints202503.0667.v1

6. Conclusions

In conclusion, perylene diimide (PDI) derivatives have emerged as pivotal players in the realm of biomedical applications, thanks to their remarkable photophysical properties and versatility in functionalization. Their exceptional fluorescence characteristics facilitate advancements in bioimaging, allowing for high-resolution visualization of biological processes and improved diagnostic capabilities. Moreover, the ability of PDI-based materials to be engineered for targeted drug delivery systems enhances the therapeutic potential of various substances while minimizing adverse effects. The involvement of PDI in photodynamic therapy (PDT) and photothermal therapy (PTT) illustrates its dual function as both a therapeutic agent and an imaging marker, offering innovative strategies for cancer treatment that combine diagnosis and therapy in a synergistic manner.

7. Future Directions

As we look to the future, several directions for research and development involving PDI can be envisaged. First, the continuous exploration of novel synthesis strategies to enhance the water solubility and biocompatibility of PDI derivatives will be crucial. This advancement will likely facilitate their incorporation into biological systems and further expand their applications in complex biological environments. Additionally, investigating the integration of PDI with emerging nanotechnologies could lead to even greater efficiencies in drug delivery systems, particularly through the development of smart nanoparticles capable of responding to environmental stimuli.

Furthermore, the exploration of new composite materials that marry PDI with other functional biomolecules or therapeutic agents could catalyze breakthroughs in targeted therapy, harnessing synergetic effects to enhance efficacy while reducing potential side effects. Lastly, clinical trials and translational research are essential to validate the safety and effectiveness of PDI-derived compounds in real-world applications. With these future directions, the full potential of perylene diimide in biomedical contexts can be realized, paving the way for innovative diagnostic and therapeutic solutions for various diseases, including cancer.

Funding: This research received no external funding.

Institutional Review Board Statement: Not applicable.

Informed Consent Statement: Not applicable.

Data Availability Statement: No new data were created or analyzed in this study.

Acknowledgments: PPK shows sincere gratitude to Department of Biomedical Engineering, Michigan State university, for the facilities and use of resources for the literature collections.

Conflicts of Interest: The author declare no conflict of interest.

References

1. Chen, S.; Xue, Z.; Gao, N.; Yang, X.; Zang, L. Perylene Diimide-Based Fluorescent and Colorimetric Sensors for Environmental Detection. *Sensors* **2020**, *20*, 917, doi:10.3390/s20030917.
2. Krupka, O.; Hudhomme, P. Recent Advances in Applications of Fluorescent Perylenediimide and Perylenemonoimide Dyes in Bioimaging, Photothermal and Photodynamic Therapy. *Int. J. Mol. Sci.* **2023**, *24*, 6308, doi:10.3390/ijms24076308.
3. Chen, S.; Zhou, M.; Zhu, L.; Yang, X.; Zang, L. Architectures and Mechanisms of Perylene Diimide-Based Optical Chemosensors for pH Probing. *Chemosensors* **2023**, *11*, 293, doi:10.3390/chemosensors11050293.
4. Soh, N.; Ueda, T. Perylene Bisimide as a Versatile Fluorescent Tool for Environmental and Biological Analysis: A Review. *Talanta* **2011**, *85*, 1233–1237, doi:10.1016/j.talanta.2011.06.010.
5. Liu, K.; Xu, Z.; Yin, M. Perylenediimide-Cored Dendrimers and Their Bioimaging and Gene Delivery Applications. *Prog. Polym. Sci.* **2015**, *46*, 25–54, doi:10.1016/j.progpolymsci.2014.11.005.

 doi:10.20944/preprints202503.0667.v1

6. Zhao, Z.; Xu, N.; Wang, Y.; Ling, G.; Zhang, P. Perylene Diimide-Based Treatment and Diagnosis of Diseases. *J. Mater. Chem. B* **2021**, *9*, 8937–8950, doi:10.1039/D1TB01752G.
7. Sun, M.; Müllen, K.; Yin, M. Water-Soluble Perylenediimides: Design Concepts and Biological Applications. *Chem. Soc. Rev.* **2016**, *45*, 1513–1528, doi:10.1039/C5CS00754B.
8. Zhao, Y.; Zhang, X.; Li, D.; Liu, D.; Jiang, W.; Han, C.; Shi, Z. Water-soluble 3,4:9,10-perylene Tetracarboxylic Ammonium as a High-performance Fluorochrome for Living Cells Staining. *Luminescence* **2009**, *24*, 140–143, doi:10.1002/bio.1078.
9. Zhou, W.; He, D.D.; Zhang, K.; Liu, N.; Li, Y.; Han, W.; Zhou, W.; Li, M.; Zhang, S.; Huang, H.; et al. A Perylene Diimide Probe for NIR-II Fluorescence Imaging Guided Photothermal and Type I/Type II Photodynamic Synergistic Therapy. *Biosens. Bioelectron.* **2024**, *259*, 116424, doi:10.1016/j.bios.2024.116424.
10. Özçil, F.; Yükrük, F. Evaluation of Singlet Oxygen Generators of Novel Water-Soluble Perylene Diimide Photosensitizers. *RSC Adv.* **2023**, *13*, 15416–15420, doi:10.1039/D3RA02338A.
11. Sun, H.; Zhang, Q. Recent Advances in Perylene Diimides (PDI)-based Small Molecules Used for Emission and Photothermal Conversion. *Chem.Photo.Chem.* **2024**, *8*, e202300213, doi:10.1002/cptc.202300213.
12. Cheng, H.; Qu, B.; Qian, C.; Xu, M.; Zhang, R. Synthesis, Fluorescence Property and Cell Imaging of a Perylene Diimide-Based NIR Fluorescent Probe for Hypochlorite with Dual-Emission Fluorescence Responses. *Mater. Adv.* **2020**, *1*, 814–819, doi:10.1039/D0MA00131G.
13. Görl, D.; Zhang, X.; Würthner, F. Molecular Assemblies of Perylene Bisimide Dyes in Water. *Angew. Chem. Int. Ed.* **2012**, *51*, 6328–6348, doi:10.1002/anie.201108690.
14. Laine, R.F.; Sinnige, T.; Ma, K.Y.; Haack, A.J.; Poudel, C.; Gaida, P.; Curry, N.; Perni, M.; Nollen, E.A.A.; Dobson, C.M.; et al. Fast Fluorescence Lifetime Imaging Reveals the Aggregation Processes of α-Synuclein and Polyglutamine in Aging *Caenorhabditis Elegans*. *ACS Chem. Biol.* **2019**, *14*, 1628–1636, doi:10.1021/acschembio.9b00354.
15. Su, P.; Ran, G.; Wang, H.; Yue, J.; Kong, Q.; Bo, Z.; Zhang, W. Intramolecular and Intermolecular Interaction Switching in the Aggregates of Perylene Diimide Trimer: Effect of Hydrophobicity. *Molecules* **2023**, *28*, 3003, doi:10.3390/molecules28073003.
16. Cho, J.; Keum, C.; Lee, S.-G.; Lee, S.-Y. Aggregation-Driven Fluorescence Quenching of Imidazole-Functionalized Perylene Diimide for Urea Sensing. *Analyst* **2020**, *145*, 7312–7319, doi:10.1039/D0AN01252A.
17. Hu, Y.; Wang, K.; Wang, Y.; Ma, L. Perylene Imide Derivatives: Structural Modification of Imide Position, Aggregation Caused Quenching Mechanism, Light-Conversion Quality and Photostability. *Dyes and Pigments* **2023**, *210*, 110948, doi:10.1016/j.dyepig.2022.110948.
18. Wu, J.; Peng, M.; Mu, M.; Li, J.; Yin, M. Perylene Diimide Supramolecular Aggregates: Constructions and Sensing Applications. *Supramol. Mater.* **2023**, *2*, 100031, doi:10.1016/j.supmat.2023.100031.
19. Rostami-Tapeh-Esmail, E.; Golshan, M.; Salami-Kalajahi, M.; Roghani-Mamaqani, H. Perylene-3,4,9,10-Tetracarboxylic Diimide and Its Derivatives: Synthesis, Properties and Bioapplications. *Dyes and Pigments* **2020**, *180*, 108488, doi:10.1016/j.dyepig.2020.108488.
20. Nowak-Król, A.; Würthner, F. Progress in the Synthesis of Perylene Bisimide Dyes. *Org. Chem. Front.* **2019**, *6*, 1272–1318, doi:10.1039/C8QO01368C.
21. Kardos, M. Über Einige Aceanthrenchinon- Und 1.9-Anthracen-Derivate. *Ber. Dtsch. Chem. Ges.* **1913**, *46*, 2086–2091, doi:10.1002/cber.191304602126.
22. Langhals, H. Cyclic Carboxylic Imide Structures as Structure Elements of High Stability. Novel Developments in Perylene Dye Chemistry. *HETEROCYCLES* **1995**, *40*, 477, doi:10.3987/REV-94-SR2.
23. Langhals, H. Synthese von Hochreinen Perylen-Fluoreszenzfarbstoffen in Großen Mengen – Gezielte Darstellung von Atrop-Isomeren. *Chem. Ber.* **1985**, *118*, 4641–4645, doi:10.1002/cber.19851181138.
24. Würthner, F. Perylene Bisimide Dyes as Versatile Building Blocks for Functional Supramolecular Architectures. *Chem. Commun.* **2004**, 1564–1579, doi:10.1039/B401630K.
25. Fukuzumi, S.; Ohkubo, K.; Ortiz, J.; Gutiérrez, A.M.; Fernández-Lázaro, F.; Sastre-Santos, Á. Formation of a Long-Lived Charge-Separated State of a Zinc Phthalocyanine-Perylenediimide Dyad by Complexation with Magnesium Ion. *Chem. Commun.* **2005**, 3814, doi:10.1039/b506412k.
26. Nagao, Y. Synthesis and Properties of Perylene Pigments. *Prog. Org. Coat.* **1997**, *31*, 43–49, doi:10.1016/S0300-9440(97)00017-9.

 doi:10.20944/preprints202503.0667.v1

27. Wicklein, A.; Kohn, P.; Ghazaryan, L.; Thurn-Albrecht, T.; Thelakkat, M. Synthesis and Structure Elucidation of Discotic Liquid Crystalline Perylene Imide Benzimidazole. *Chem. Commun.* **2010**, *46*, 2328, doi:10.1039/b921476c.
28. Iverson, I.K.; Tam-Chang, S.-W. Cascade of Molecular Order by Sequential Self-Organization, Induced Orientation, and Order Transfer Processes. *J. Am. Chem. Soc.* **1999**, *121*, 5801–5802, doi:10.1021/ja983803j.
29. Sommer, M.; Lindner, S.M.; Thelakkat, M. Microphase-Separated Donor–Acceptor Diblock Copolymers: Influence of HOMO Energy Levels and Morphology on Polymer Solar Cells. *Adv. Funct. Mater.* **2007**, *17*, 1493–1500, doi:10.1002/adfm.200600634.
30. Sommer, M.; Lang, A.S.; Thelakkat, M. Crystalline–Crystalline Donor–Acceptor Block Copolymers. *Angew. Chem. Int. Ed.* **2008**, *47*, 7901–7904, doi:10.1002/anie.200802725.
31. Lindner, S.M.; Hüttner, S.; Chiche, A.; Thelakkat, M.; Krausch, G. Charge Separation at Self-Assembled Nanostructured Bulk Interface in Block Copolymers. *Angew. Chem. Int. Ed.* **2006**, *45*, 3364–3368, doi:10.1002/anie.200503958.
32. Kwakernaak, M.C.; Koel, M.; Van Den Berg, P.J.L.; Kelder, E.M.; Jager, W.F. Room Temperature Synthesis of Perylene Diimides Facilitated by High Amic Acid Solubility. *Org. Chem. Front.* **2022**, *9*, 1090–1108, doi:10.1039/D1QO01723C.
33. Kelber, J.; Bock, H.; Thiebaut, O.; Grelet, E.; Langhals, H. Room-Temperature Columnar Liquid-Crystalline Perylene Imido-Diesters by a Homogeneous One-Pot Imidification–Esterification of Perylene-3,4,9,10-tetracarboxylic Dianhydride. *Eur. J. Org. Chem.* **2011**, *2011*, 707–712, doi:10.1002/ejoc.201001346.
34. Dubey, R.K.; Westerveld, N.; Grozema, F.C.; Sudhölter, E.J.R.; Jager, W.F. Facile Synthesis of Pure 1,6,7,12-Tetrachloroperylene-3,4,9,10-Tetracarboxy Bisanhydride and Bisimide. *Org. Lett.* **2015**, *17*, 1882–1885, doi:10.1021/acs.orglett.5b00562.
35. Baumgartner, B.; Svirkova, A.; Bintinger, J.; Hametner, C.; Marchetti-Deschmann, M.; Unterlass, M.M. Green and Highly Efficient Synthesis of Perylene and Naphthalene Bisimides in Nothing but Water. *Chem. Commun.* **2017**, *53*, 1229–1232, doi:10.1039/C6CC06567H.
36. Cao, Q.; Crawford, D.E.; Shi, C.; James, S.L. Greener Dye Synthesis: Continuous, Solvent-Free Synthesis of Commodity Perylene Diimides by Twin-Screw Extrusion. *Angew. Chem. Int. Ed.* **2020**, *59*, 4478–4483, doi:10.1002/anie.201913625.
37. Moura, H.M.; Peterlik, H.; Unterlass, M.M. Green Hydrothermal Synthesis Yields Perylenebisimide–SiO_2 Hybrid Materials with Solution-like Fluorescence and Photoredox Activity. *J. Mater. Chem. A* **2022**, *10*, 12817–12831, doi:10.1039/D1TA03214C.
38. Wang, H.Z.; Ning, L.G.; Lv, W.Y.; Xiao, L.; Li, C.M.; Lu, Z.S.; Wang, B.; Xu, L.Q. Green Synthesis of Perylene Diimide-Based Nanodots for Carbon Dioxide Sensing, Antibacterial Activity Prediction and Bacterial Discrimination. *Dyes and Pigments* **2020**, *176*, 108245, doi:10.1016/j.dyepig.2020.108245.
39. Aivali, S.; Tsimpouki, L.; Anastasopoulos, C.; Kallitsis, J.K. Synthesis and Optoelectronic Characterization of Perylene Diimide-Quinoline Based Small Molecules. *Molecules* **2019**, *24*, 4406, doi:10.3390/molecules24234406.
40. Zhang, J.; Singh, S.; Hwang, D.K.; Barlow, S.; Kippelen, B.; Marder, S.R. 2-Bromo Perylene Diimide: Synthesis Using C–H Activation and Use in the Synthesis of Bis(Perylene Diimide)–Donor Electron-Transport Materials. *J. Mater. Chem. C* **2013**, *1*, 5093, doi:10.1039/c3tc30918e.
41. Ganesamoorthy, R.; Vijayaraghavan, R.; Ramki, K.; Sakthivel, P. Synthesis, Characterization of Bay-Substituted Perylene Diimide Based D-A-D Type Small Molecules and Their Applications as a Non-Fullerene Electron Acceptor in Polymer Solar Cells. *J. Sci.: Adv. Mater. Devices.* **2018**, *3*, 99–106, doi:10.1016/j.jsamd.2017.11.005.
42. Siddiqui, A.; Thawarkar, S.; Singh, S.P. A Novel Perylenediimide Molecule: Synthesis, Structural Property Relationship and Nanoarchitectonics. *J. Solid State Chem.* **2022**, *306*, 122687, doi:10.1016/j.jssc.2021.122687.
43. Qiu, W.; Chen, S.; Sun, X.; Liu, Y.; Zhu, D. Suzuki Coupling Reaction of 1,6,7,12-Tetrabromoperylene Bisimide. *Org. Lett.* **2006**, *8*, 867–870, doi:10.1021/ol052923a.
44. El-Berjawi, R.; Hudhomme, P. Synthesis of a Perylenediimide-Fullerene C60 Dyad: A Simple Use of a Nitro Leaving Group for a Suzuki-Miyaura Coupling Reaction. *Dyes and Pigments* **2018**, *159*, 551–556, doi:10.1016/j.dyepig.2018.07.037.

 doi:10.20944/preprints202503.0667.v1

45. Li, A.; Zhang, X.; Wang, S.; Wei, K.; Du, P. Synthesis and Physical Properties of a Perylene Diimide-Embedded Chiral Conjugated Macrocycle. *Org. Lett.* **2023**, *25*, 1183–1187, doi:10.1021/acs.orglett.3c00152.
46. Kuklin, S.A.; Safronov, S.V.; Khakina, E.A.; Buyanovskaya, A.G.; Frolova, L.A.; Troshin, P.A. New Perylene Diimide Electron Acceptors for Organic Electronics: Synthesis, Optoelectronic Properties and Performance in Perovskite Solar Cells. *Mendeleev Communications* **2023**, *33*, 314–317, doi:10.1016/j.mencom.2023.04.005.
47. Huo, L.; Zhou, Y.; Li, Y. Synthesis and Absorption Spectra of n-Type Conjugated Polymers Based on Perylene Diimide. *Macromol. Rapid Commun.* **2008**, *29*, 1444–1448, doi:10.1002/marc.200800268.
48. Feng, J.; Jiang, W.; Wang, Z. Synthesis and Application of Rylene Imide Dyes as Organic Semiconducting Materials. *Chem. Asian J.* **2018**, *13*, 20–30, doi:10.1002/asia.201701424.
49. Wang, L.-H.; Liu, L.-L.; Liu, H.; Chen, Y.; Ye, D.-N.; Fu, W.; Liu, S.-Y. Diketopyrrolopyrrole and Perylene Diimine-Based Large π-Molecules Constructed via C–H Direct Arylation. *Dyes and Pigments* **2022**, *204*, 110468, doi:10.1016/j.dyepig.2022.110468.
50. Hoffman, E.; Kozakiewicz, K.; Rybczyńska, M.; Mońka, M.; Grzywacz, D.; Liberek, B.; Bojarski, P.; Serdiuk, I.E. Photochemical Transformation of a Perylene Diimide Derivative Beneficial for the *in Situ* Formation of a Molecular Photocatalyst of the Hydrogen Evolution Reaction. *J. Mater. Chem. A* **2024**, *12*, 5233–5243, doi:10.1039/D3TA05930H.
51. Zhang, F.; Ma, Y.; Chi, Y.; Yu, H.; Li, Y.; Jiang, T.; Wei, X.; Shi, J. Self-Assembly, Optical and Electrical Properties of Perylene Diimide Dyes Bearing Unsymmetrical Substituents at Bay Position. *Sci. Rep.* **2018**, *8*, 8208, doi:10.1038/s41598-018-26502-5.
52. Kim, H.J.; Lee, C.; Schuck, P.J.; Kaufman, L.J. Aggregation Pathway Complexity in a Simple Perylene Diimide. *Sci Rep* **2024**, *14*, 31989, doi:10.1038/s41598-024-83525-x.
53. Almuhana, A.R.Y.; Langer, P.; Griffin, S.L.; Lodge, R.W.; Rance, G.A.; Champness, N.R. Retention of Perylene Diimide Optical Properties in Solid-State Materials through Tethering to Nanodiamonds. *J. Mater. Chem. C* **2021**, *9*, 10317–10323, doi:10.1039/D1TC02577E.
54. He, J.; Li, S.; Zeng, H. The Photostability of Two Optical Materials Based on Perylene Diimide Substituted by Different Aromatic Groups at the Bay Area. *J. Heterocyclic Chem.* **2017**, *54*, 2800–2807, doi:10.1002/jhet.2883.
55. Asir, S.; Zanardi, C.; Seeber, R.; Icil, H. A Novel Unsymmetrically Substituted Chiral Amphiphilic Perylene Diimide: Synthesis, Photophysical and Electrochemical Properties Both in Solution and Solid State. *J. Photochem. Photobiol. C Photochem. Rev.* **2016**, *318*, 104–113, doi:10.1016/j.jphotochem.2015.12.008.
56. Chao, C.-C.; Leung, M.; Su, Y.O.; Chiu, K.-Y.; Lin, T.-H.; Shieh, S.-J.; Lin, S.-C. Photophysical and Electrochemical Properties of 1,7-Diaryl-Substituted Perylene Diimides. *J. Org. Chem.* **2005**, *70*, 4323–4331, doi:10.1021/jo050001f.
57. Tang, N.; Zhou, J.; Wang, L.; Stolte, M.; Xie, G.; Wen, X.; Liu, L.; Würthner, F.; Gierschner, J.; Xie, Z. Anomalous Deep-Red Luminescence of Perylene Black Analogues with Strong π-π Interactions. *Nat. Commun.* **2023**, *14*, 1922, doi:10.1038/s41467-023-37171-y.
58. Al-Khateeb, B.; Dinleyici, M.; Abourajab, A.; Kök, C.; Bodapati, J.B.; Uzun, D.; Koyuncu, S.; Icil, H. Swallow Tail Bay-Substituted Novel Perylene Bisimides: Synthesis, Characterization, Photophysical and Electrochemical Properties and DFT Studies. *J. Photochem. Photobiol. A. Chem.* **2020**, *393*, 112432, doi:10.1016/j.jphotochem.2020.112432.
59. Das, L.; Das, P.; Ahamed, S.M.; Datta, A.; Pal, A.K.; Datta, A.; Malik, S. Bay-Substituted Perylene Diimide-Based Donor–Acceptor Type Copolymers: Design, Synthesis, Optical and Energy Storage Behaviours. *J. Mater. Chem. A* **2025**, *13*, 1842–1852, doi:10.1039/D4TA06278G.
60. Vajiravelu, S.; Ramunas, L.; Juozas Vidas, G.; Valentas, G.; Vygintas, J.; Valiyaveettil, S. Effect of Substituents on the Electron Transport Properties of Bay Substituted Perylene Diimide Derivatives. *J. Mater. Chem.* **2009**, *19*, 4268, doi:10.1039/b901847f.
61. Yang, S.K.; Zimmerman, S.C. Polyglycerol-Dendronized Perylenediimides as Stable, Water-Soluble Fluorophores. *Adv. Funct. Mater.* **2012**, *22*, 3023–3028, doi:10.1002/adfm.201200004.
62. Battagliarin, G.; Davies, M.; Mackowiak, S.; Li, C.; Müllen, K. *Ortho* -Functionalized Perylenediimides for Highly Fluorescent Water-Soluble Dyes. *Chem. Phys. Chem.* **2012**, *13*, 923–926, doi:10.1002/cphc.201100833.

 doi:10.20944/preprints202503.0667.v1

63. Qu, J.; Kohl, C.; Pottek, M.; Müllen, K. Ionic Perylenetetracarboxdiimides: Highly Fluorescent and Water-Soluble Dyes for Biolabeling. *Angew. Chem. Int. Ed.* **2004**, *43*, 1528–1531, doi:10.1002/anie.200353208.
64. Kohl, C.; Weil, T.; Qu, J.; Müllen, K. Towards Highly Fluorescent and Water-Soluble Perylene Dyes. *Chem. Eur. J.* **2004**, *10*, 5297–5310, doi:10.1002/chem.200400291.
65. Yukruk, F.; Dogan, A.L.; Canpinar, H.; Guc, D.; Akkaya, E.U. Water-Soluble Green Perylenediimide (PDI) Dyes as Potential Sensitizers for Photodynamic Therapy. *Org. Lett.* **2005**, *7*, 2885–2887, doi:10.1021/ol050841g.
66. Draper, E.R.; Walsh, J.J.; McDonald, T.O.; Zwijnenburg, M.A.; Cameron, P.J.; Cowan, A.J.; Adams, D.J. Air-Stable Photoconductive Films Formed from Perylene Bisimide Gelators. *J. Mater. Chem. C* **2014**, *2*, 5570–5575, doi:10.1039/C4TC00744A.
67. Kozma, E.; Grisci, G.; Mróz, W.; Catellani, M.; Eckstein-Andicsovà, A.; Pagano, K.; Galeotti, F. Water-Soluble Aminoacid Functionalized Perylene Diimides: The Effect of Aggregation on the Optical Properties in Organic and Aqueous Media. *Dyes and Pigments* **2016**, *125*, 201–209, doi:10.1016/j.dyepig.2015.10.019.
68. Heek, T.; Fasting, C.; Rest, C.; Zhang, X.; Würthner, F.; Haag, R. Highly Fluorescent Water-Soluble Polyglycerol-Dendronized Perylene Bisimide Dyes. *Chem. Commun.* **2010**, *46*, 1884–1886, doi:10.1039/B923806A.
69. You, S.; Cai, Q.; Müllen, K.; Yang, W.; Yin, M. pH-Sensitive Unimolecular Fluorescent Polymeric Micelles: From Volume Phase Transition to Optical Response. *Chem. Commun.* **2014**, *50*, 823–825, doi:10.1039/C3CC48046A.
70. Yin, M.; Feng, C.; Shen, J.; Yu, Y.; Xu, Z.; Yang, W.; Knoll, W.; Müllen, K. Dual-Responsive Interaction to Detect DNA on Template-Based Fluorescent Nanotubes. *Small* **2011**, *7*, 1629–1634, doi:10.1002/smll.201100187.
71. Yin, M.; Shen, J.; Gropeanu, R.; Pflugfelder, G.O.; Weil, T.; Müllen, K. Fluorescent Core/Shell Nanoparticles for Specific Cell-Nucleus Staining. *Small* **2008**, *4*, 894–898, doi:10.1002/smll.200701107.
72. Wang, B.; Yu, C. Fluorescence Turn-On Detection of a Protein through the Reduced Aggregation of a Perylene Probe. *Angew. Chem. Int. Ed.* **2010**, *49*, 1485–1488, doi:10.1002/anie.200905237.
73. Xu, Z.; Cheng, W.; Guo, K.; Yu, J.; Shen, J.; Tang, J.; Yang, W.; Yin, M. Molecular Size, Shape, and Electric Charges: Essential for Perylene Bisimide-Based DNA Intercalator to Localize in Cell Nuclei and Inhibit Cancer Cell Growth. *ACS Appl. Mater. Interfaces* **2015**, *7*, 9784–9791, doi:10.1021/acsami.5b01665.
74. You, S.; Cai, Q.; Zheng, Y.; He, B.; Shen, J.; Yang, W.; Yin, M. Perylene-Cored Star-Shaped Polycations for Fluorescent Gene Vectors and Bioimaging. *ACS Appl. Mater. Interfaces* **2014**, *6*, 16327–16334, doi:10.1021/am5045967.
75. Gryszel, M.; Schlossarek, T.; Würthner, F.; Natali, M.; Głowacki, E.D. Water-Soluble Cationic Perylene Diimide Dyes as Stable Photocatalysts for H_2 O_2 Evolution. *Chem.Photo.Chem.* **2023**, *7*, e202300070, doi:10.1002/cptc.202300070.
76. Bag, K.; Halder, R.; Jana, B.; Malik, S. Solvent-Assisted Enhanced Emission of Cationic Perylene Diimide Supramolecular Assembly in Water: A Perspective from Experiment and Simulation. *J. Phys. Chem. C* **2019**, *123*, 6241–6249, doi:10.1021/acs.jpcc.8b11054.
77. Xu, Z.; He, B.; Wei, W.; Liu, K.; Yin, M.; Yang, W.; Shen, J. Highly Water-Soluble Perylenediimide-Cored Poly(Amido Amine) Vector for Efficient Gene Transfection. *J. Mater. Chem. B* **2014**, *2*, 3079–3086, doi:10.1039/C4TB00195H.
78. Gao, B.; Li, H.; Liu, H.; Zhang, L.; Bai, Q.; Ba, X. Water-Soluble and Fluorescent Dendritic Perylene Bisimides for Live-Cell Imaging. *Chem. Commun.* **2011**, *47*, 3894, doi:10.1039/c1cc00058f.
79. Bo, F.; Gao, B.; Duan, W.; Li, H.; Liu, H.; Bai, Q. Assembly–Disassembly Driven "off–on" Fluorescent Perylene Bisimide Probes for Detecting and Tracking of Proteins in Living Cells. *RSC Adv.* **2013**, *3*, 17007, doi:10.1039/c3ra42284d.
80. Yang, S.K.; Shi, X.; Park, S.; Doganay, S.; Ha, T.; Zimmerman, S.C. Monovalent, Clickable, Uncharged, Water-Soluble Perylenediimide-Cored Dendrimers for Target-Specific Fluorescent Biolabeling. *J. Am. Chem. Soc.* **2011**, *133*, 9964–9967, doi:10.1021/ja2009136.
81. Singh, P.; Hirsch, A.; Kumar, S. Perylene Diimide-Based Chemosensors Emerging in Recent Years: From Design to Sensing. *Trends Anal. Chem.* **2021**, *138*, 116237, doi:10.1016/j.trac.2021.116237.

 doi:10.20944/preprints202503.0667.v1

82. Kaur, N.; Kour, R.; Kaur, S.; Singh, P. Perylene Diimide-Based Sensors for Multiple Analyte Sensing (Fe^{2+} /H_2 S/ Dopamine and Hg^{2+} /Fe^{2+}): Cell Imaging and INH, XOR, and Encoder Logic. *Anal. Methods* **2023**, *15*, 2391–2398, doi:10.1039/D3AY00290J.
83. Zhao, J.; Huang, R.; Gao, Y.; Xu, J.; Sun, Y.; Bao, J.; Fang, L.; Gou, S. Realizing Near-Infrared (NIR)-Triggered Type-I PDT and PTT by Maximizing the Electronic Exchange Energy of Perylene Diimide-Based Photosensitizers. *ACS Materials Lett.* **2023**, *5*, 1752–1759, doi:10.1021/acsmaterialslett.3c00436.
84. Yan, L.; Ye, Z.; Peng, C.; Zhang, S. A New Perylene Diimide-Based Fluorescent Chemosensor for Selective Detection of ATP in Aqueous Solution. *Tetrahedron* **2012**, *68*, 2725–2727, doi:10.1016/j.tet.2012.01.028.
85. Lv, Z.; Liu, J.; Bai, W.; Yang, S.; Chen, A. A Simple and Sensitive Label-Free Fluorescent Approach for Protein Detection Based on a Perylene Probe and Aptamer. *Biosens. Bioelectron.* **2015**, *64*, 530–534, doi:10.1016/j.bios.2014.09.095.
86. Zong, L.; Zhang, H.; Li, Y.; Gong, Y.; Li, D.; Wang, J.; Wang, Z.; Xie, Y.; Han, M.; Peng, Q.; et al. Tunable Aggregation-Induced Emission Nanoparticles by Varying Isolation Groups in Perylene Diimide Derivatives and Application in Three-Photon Fluorescence Bioimaging. *ACS Nano* **2018**, *12*, 9532–9540, doi:10.1021/acsnano.8b05090.
87. Ma, Y.; Zhang, F.; Zhang, J.; Jiang, T.; Li, X.; Wu, J.; Ren, H. A Water-soluble Fluorescent pH Probe Based on Perylene Dyes and Its Application to Cell Imaging. *Luminescence* **2016**, *31*, 102–107, doi:10.1002/bio.2930.
88. Jana, A.; Nguyen, K.T.; Li, X.; Zhu, P.; Tan, N.S.; Ågren, H.; Zhao, Y. Perylene-Derived Single-Component Organic Nanoparticles with Tunable Emission: Efficient Anticancer Drug Carriers with Real-Time Monitoring of Drug Release. *ACS Nano* **2014**, *8*, 5939–5952, doi:10.1021/nn501073x.
89. Jana, A.; Devi, K.S.P.; Maiti, T.K.; Singh, N.D.P. Perylene-3-Ylmethanol: Fluorescent Organic Nanoparticles as a Single-Component Photoresponsive Nanocarrier with Real-Time Monitoring of Anticancer Drug Release. *J. Am. Chem. Soc.* **2012**, *134*, 7656–7659, doi:10.1021/ja302482k.
90. Cheng, W.; Chen, H.; Ji, C.; Yang, R.; Yin, M. A Perylenediimide-Based Nanocarrier Monitors Curcumin Release with an "off–on" Fluorescence Switch. *Polym. Chem.* **2019**, *10*, 2551–2558, doi:10.1039/C9PY00132H.
91. Zhou, P.; Aschauer, U.; Decurtins, S.; Feurer, T.; Häner, R.; Liu, S.-X. Merging of Azulene and Perylene Diimide for Optical pH Sensors. *Molecules* **2023**, *28*, 6694, doi:10.3390/molecules28186694.
92. Tariq, A.; Garnier, U.; Ghasemi, R.; Pierre Lefevre, J.; Mongin, C.; Brosseau, A.; Frédéric Audibert, J.; Pansu, Robert.; Dauzères, A.; Leray, I. Perylene Based PET Fluorescent Molecular Probes for pH Monitoring. *J. Photochem. Photobiol. A. Chem.* **2022**, *432*, 114035, doi:10.1016/j.jphotochem.2022.114035.
93. Georgiev, N.I.; Said, A.I.; Toshkova, R.A.; Tzoneva, R.D.; Bojinov, V.B. A Novel Water-Soluble Perylenetetracarboxylic Diimide as a Fluorescent pH Probe: Chemosensing, Biocompatibility and Cell Imaging. *Dyes and Pigments* **2019**, *160*, 28–36, doi:10.1016/j.dyepig.2018.07.048.
94. Chen, Y.; Liu, W.; Zhang, B.; Suo, Z.; Xing, F.; Feng, L. Sensitive and Reversible Perylene Derivative-Based Fluorescent Probe for Acetylcholinesterase Activity Monitoring and Its Inhibitor. *Anal. Biochem.* **2020**, *607*, 113835, doi:10.1016/j.ab.2020.113835.
95. Muthuraj, B.; Mukherjee, S.; Chowdhury, S.R.; Patra, C.R.; Iyer, P.K. An Efficient Strategy to Assemble Water Soluble Histidine-Perylene Diimide and Graphene Oxide for the Detection of PPi in Physiological Conditions and in Vitro. *Biosens. Bioelectron.* **2017**, *89*, 636–644, doi:10.1016/j.bios.2015.12.036.
96. Dey, S.; Sukul, P.Kr. Selective Detection of Pyrophosphate Anions in Aqueous Medium Using Aggregation of Perylene Diimide as a Fluorescent Probe. *ACS Omega* **2019**, *4*, 16191–16200, doi:10.1021/acsomega.9b02405.
97. Feng, C.L.; Yin, M.; Zhang, D.; Zhu, S.; Caminade, A.M.; Majoral, J.P.; Müllen, K. Fluorescent Core-Shell Star Polymers Based Bioassays for Ultrasensitive DNA Detection by Surface Plasmon Fluorescence Spectroscopy. *Macromol. Rapid Commun.* **2011**, *32*, 679–683, doi:10.1002/marc.201000788.
98. Feng, X.; An, Y.; Yao, Z.; Li, C.; Shi, G. A Turn-on Fluorescent Sensor for Pyrophosphate Based on the Disassembly of Cu^{2+} -Mediated Perylene Diimide Aggregates. *ACS Appl. Mater. Interfaces* **2012**, *4*, 614–618, doi:10.1021/am201616r.
99. Wang, K.-R.; Wang, Y.-Q.; Li, J.; An, H.-W.; Zhang, L.-P.; Zhang, J.-C.; Li, X.-L. Synthesis of Perylene Bisimide-Centered Glycodendrimer and Its Interactions with Concanavalin A. *Bioorg. Med. Chem. Lett.* **2013**, *23*, 480–483, doi:10.1016/j.bmcl.2012.11.049.

 doi:10.20944/preprints202503.0667.v1

100. Wang, K.-R.; An, H.-W.; Qian, F.; Wang, Y.-Q.; Zhang, J.-C.; Li, X.-L. Synthesis, Optical Properties and Binding Interactions of a Multivalent Glycocluster Based on a Fluorescent Perylene Bisimide Derivative. *RSC Adv.* **2013**, *3*, 23190, doi:10.1039/c3ra44675a.
101. Hao, Y.; Zhu, X.; Dong, Y.; Zhang, N.; Wang, H.; Li, X.; Ren, X.; Ma, H.; Wei, Q. Self-Assembled Perylene Diimide (PDI) Nanowire Sensitized In_2O_3@$MgIn_2S_4$ S-Scheme Heterojunction as Photoelectrochemical Biosensing Platform for the Detection of CA15–3. *Anal. Chem.* **2024**, *96*, 13197–13206, doi:10.1021/acs.analchem.4c02179.
102. Yadav, S.; Choudhary, N.; Vasave, A.T.; Sonpal, V.; Paital, A.R. Perylene Diimide Functionalized Nano-Silica: Green Emissive Material for Selective Probing and Remediation of 4-Nitrocatechol, Ru^{3+} , and Cu^{2+} with Biosensing Applications. *Mater. Adv.* **2024**, *5*, 8937–8952, doi:10.1039/D4MA00862F.
103. Zhou, J.; Zhang, J.; Lai, Y.; Zhou, Z.; Zhao, Y.; Wang, H.; Wang, Z. Guanidinium-Dendronized Perylene Bisimides as Stable, Water-Soluble Fluorophores for Live-Cell Imaging. *New J. Chem.* **2013**, *37*, 2983, doi:10.1039/c3nj00876b.
104. Yin, M.; Kuhlmann, C.R.W.; Sorokina, K.; Li, C.; Mihov, G.; Pietrowski, E.; Koynov, K.; Klapper, M.; Luhmann, H.J.; Weil, T. Novel Fluorescent Core–Shell Nanocontainers for Cell Membrane Transport. *Biomacromolecules* **2008**, *9*, 1381–1389, doi:10.1021/bm701138g.
105. Heek, T.; Nikolaus, J.; Schwarzer, R.; Fasting, C.; Welker, P.; Licha, K.; Herrmann, A.; Haag, R. An Amphiphilic Perylene Imido Diester for Selective Cellular Imaging. *Bioconjugate Chem.* **2013**, *24*, 153–158, doi:10.1021/bc3005655.
106. Cui, X.; Shi, B.; Qiu, Z.; Yang, F.; Wang, X.; Xu, Y.; Wei, W. Highly Fluorescent, Water-Soluble Tetrapodal Perylene Diimides Insulated by Cationic Pendants for Live-Cell Imaging. *Dyes and Pigments* **2025**, *232*, 112460, doi:10.1016/j.dyepig.2024.112460.
107. Yang, Z.; Li, X.; Sun, T.; Bian, J.; Bu, X.; Ge, X.; Sun, J.; Liu, Z.; Xie, Z.; Xi, P.; et al. Multicolor Tuning of Perylene Diimides Dyes for Targeted Organelle Imaging In Vivo. *Anal. Chem.* **2024**, acs.analchem.4c01601, doi:10.1021/acs.analchem.4c01601.
108. Yang, F.; Li, R.; Wei, W.; Ding, X.; Xu, Z.; Wang, P.; Wang, G.; Xu, Y.; Fu, H.; Zhao, Y. Water-Soluble Doubly-Strapped Isolated Perylene Diimide Chromophore. *Angew. Chem. Int. Ed.* **2022**, *61*, e202202491, doi:10.1002/anie.202202491.
109. Casagrande, V.; Salvati, E.; Alvino, A.; Bianco, A.; Ciammaichella, A.; D'Angelo, C.; Ginnari-Satriani, L.; Serrilli, A.M.; Iachettini, S.; Leonetti, C.; et al. *N* -Cyclic Bay-Substituted Perylene G-Quadruplex Ligands Have Selective Antiproliferative Effects on Cancer Cells and Induce Telomere Damage. *J. Med. Chem.* **2011**, *54*, 1140–1156, doi:10.1021/jm1013665.
110. Kulkarni, B.; Malhotra, M.; Jayakannan, M. Perylene-Tagged Polycaprolactone Block Copolymers and Their Enzyme-Biodegradable Fluorescent Nanoassemblies for Intracellular Bio-Imaging in Cancer Cells. *ACS Appl. Polym. Mater.* **2019**, *1*, 3375–3388, doi:10.1021/acsapm.9b00800.
111. Yang, Z.; Yuan, Y.; Jiang, R.; Fu, N.; Lu, X.; Tian, C.; Hu, W.; Fan, Q.; Huang, W. Homogeneous Near-Infrared Emissive Polymeric Nanoparticles Based on Amphiphilic Diblock Copolymers with Perylene Diimide and PEG Pendants: Self-Assembly Behavior and Cellular Imaging Application. *Polym. Chem.* **2014**, *5*, 1372–1380, doi:10.1039/C3PY01197F.
112. Ye, Y.; Zheng, Y.; Ji, C.; Shen, J.; Yin, M. Self-Assembly and Disassembly of Amphiphilic Zwitterionic Perylenediimide Vesicles for Cell Membrane Imaging. *ACS Appl. Mater. Interfaces* **2017**, *9*, 4534–4539, doi:10.1021/acsami.6b15592.
113. Abdelhameed, M.; Aly, S.; Lant, J.T.; Zhang, X.; Charpentier, P. Energy/Electron Transfer Switch for Controlling Optical Properties of Silicon Quantum Dots. *Sci. Rep.* **2018**, *8*, 17068, doi:10.1038/s41598-018-35201-0.
114. Ribeiro, T.; Raja, S.; Rodrigues, A.S.; Fernandes, F.; Baleizão, C.; Farinha, J.P.S. NIR and Visible Perylenediimide-Silica Nanoparticles for Laser Scanning Bioimaging. *Dyes and Pigments* **2014**, *110*, 227–234, doi:10.1016/j.dyepig.2014.03.026.
115. Fan, Q.; Cheng, K.; Yang, Z.; Zhang, R.; Yang, M.; Hu, X.; Ma, X.; Bu, L.; Lu, X.; Xiong, X.; et al. Perylene-Diimide-Based Nanoparticles as Highly Efficient Photoacoustic Agents for Deep Brain Tumor Imaging in Living Mice. *Adv. Mater.* **2015**, *27*, 843–847, doi:10.1002/adma.201402972.

 doi:10.20944/preprints202503.0667.v1

116. Yang, Y.; Fryer, C.; Sharkey, J.; Thomas, A.; Wais, U.; Jackson, A.W.; Wilm, B.; Murray, P.; Zhang, H. Perylene Diimide Nanoprobes for In Vivo Tracking of Mesenchymal Stromal Cells Using Photoacoustic Imaging. *ACS Appl. Mater. Interfaces* **2020**, *12*, 27930–27939, doi:10.1021/acsami.0c03857.
117. Cui, C.; Yang, Z.; Hu, X.; Wu, J.; Shou, K.; Ma, H.; Jian, C.; Zhao, Y.; Qi, B.; Hu, X.; et al. Organic Semiconducting Nanoparticles as Efficient Photoacoustic Agents for Lightening Early Thrombus and Monitoring Thrombolysis in Living Mice. *ACS Nano* **2017**, *11*, 3298–3310, doi:10.1021/acsnano.7b00594.
118. Li, S.-A.; Meng, X.-Y.; Zhang, Y.-J.; Chen, C.-L.; Jiao, Y.-X.; Zhu, Y.-Q.; Liu, P.-P.; Sun, W. Progress in pH-Sensitive Sensors: Essential Tools for Organelle pH Detection, Spotlighting Mitochondrion and Diverse Applications. *Front. Pharmacol.* **2024**, *14*, 1339518, doi:10.3389/fphar.2023.1339518.
119. Ghosh, S.; Lai, J.-Y. Recent Advances in the Design of Intracellular pH Sensing Nanoprobes Based on Organic and Inorganic Materials. *Environmental Research* **2023**, *237*, 117089, doi:10.1016/j.envres.2023.117089.
120. Ma, Y.; Li, J.; Hou, S.; Zhang, J.; Shi, Z.; Jiang, T.; Wei, X. pH-Sensitive Perylene Tetra-(Alkoxycarbonyl) Probes for Live Cell Imaging. *New J. Chem.* **2016**, *40*, 6615–6622, doi:10.1039/C6NJ00153J.
121. Ye, F.; Liang, X.-M.; Wu, N.; Li, P.; Chai, Q.; Fu, Y. A New Perylene-Based Fluorescent pH Chemosensor for Strongly Acidic Condition. *Spectrochimica Acta Part A: Molecular and Biomolecular Spectroscopy* **2019**, *216*, 359–364, doi:10.1016/j.saa.2019.03.049.
122. Sun, M.; Yin, W.; Dong, X.; Yang, W.; Zhao, Y.; Yin, M. Fluorescent Supramolecular Micelles for Imaging-Guided Cancer Therapy. *Nanoscale* **2016**, *8*, 5302–5312, doi:10.1039/C6NR00450D.
123. Yang, Z.; Song, J.; Dai, Y.; Chen, J.; Wang, F.; Lin, L.; Liu, Y.; Zhang, F.; Yu, G.; Zhou, Z.; et al. Self-Assembly of Semiconducting-Plasmonic Gold Nanoparticles with Enhanced Optical Property for Photoacoustic Imaging and Photothermal Therapy. *Theranostics* **2017**, *7*, 2177–2185, doi:10.7150/thno.20545.
124. Sun, P.; Yuan, P.; Wang, G.; Deng, W.; Tian, S.; Wang, C.; Lu, X.; Huang, W.; Fan, Q. High Density Glycopolymers Functionalized Perylene Diimide Nanoparticles for Tumor-Targeted Photoacoustic Imaging and Enhanced Photothermal Therapy. *Biomacromolecules* **2017**, *18*, 3375–3386, doi:10.1021/acs.biomac.7b01029.
125. Yang, Z.; Tian, R.; Wu, J.; Fan, Q.; Yung, B.C.; Niu, G.; Jacobson, O.; Wang, Z.; Liu, G.; Yu, G.; et al. Impact of Semiconducting Perylene Diimide Nanoparticle Size on Lymph Node Mapping and Cancer Imaging. *ACS Nano* **2017**, *11*, 4247–4255, doi:10.1021/acsnano.7b01261.
126. Yang, Z.; Fan, W.; Zou, J.; Tang, W.; Li, L.; He, L.; Shen, Z.; Wang, Z.; Jacobson, O.; Aronova, M.A.; et al. Precision Cancer Theranostic Platform by In Situ Polymerization in Perylene Diimide-Hybridized Hollow Mesoporous Organosilica Nanoparticles. *J. Am. Chem. Soc.* **2019**, *141*, 14687–14698, doi:10.1021/jacs.9b06086.
127. Siafaka, P.I.; Okur, N.Ü.; Karantas, I.D.; Okur, M.E.; Gündoğdu, E.A. Current Update on Nanoplatforms as Therapeutic and Diagnostic Tools: A Review for the Materials Used as Nanotheranostics and Imaging Modalities. *Asian J. Pharm. Sci.* **2021**, *16*, 24–46, doi:10.1016/j.ajps.2020.03.003.
128. Yang, Z.; Song, J.; Tang, W.; Fan, W.; Dai, Y.; Shen, Z.; Lin, L.; Cheng, S.; Liu, Y.; Niu, G.; et al. Stimuli-Responsive Nanotheranostics for Real-Time Monitoring Drug Release by Photoacoustic Imaging. *Theranostics* **2019**, *9*, 526–536, doi:10.7150/thno.30779.
129. Yang, Z.; Dai, Y.; Yin, C.; Fan, Q.; Zhang, W.; Song, J.; Yu, G.; Tang, W.; Fan, W.; Yung, B.C.; et al. Activatable Semiconducting Theranostics: Simultaneous Generation and Ratiometric Photoacoustic Imaging of Reactive Oxygen Species In Vivo. *Adv. Mater.* **2018**, *30*, 1707509, doi:10.1002/adma.201707509.
130. Tang, W.; Yang, Z.; Wang, S.; Wang, Z.; Song, J.; Yu, G.; Fan, W.; Dai, Y.; Wang, J.; Shan, L.; et al. Organic Semiconducting Photoacoustic Nanodroplets for Laser-Activatable Ultrasound Imaging and Combinational Cancer Therapy. *ACS Nano* **2018**, *12*, 2610–2622, doi:10.1021/acsnano.7b08628.
131. Cheng, W.; Cheng, H.; Wan, S.; Zhang, X.; Yin, M. Dual-Stimulus-Responsive Fluorescent Supramolecular Prodrug for Antitumor Drug Delivery. *Chem. Mater.* **2017**, *29*, 4218–4226, doi:10.1021/acs.chemmater.7b00047.
132. Li, H.; Yue, L.; Li, L.; Liu, G.; Zhang, J.; Luo, X.; Wu, F. Triphenylamine-Perylene Diimide Conjugate-Based Organic Nanoparticles for Photoacoustic Imaging and Cancer Phototherapy. *Colloids and Surfaces B: Biointerfaces* **2021**, *205*, 111841, doi:10.1016/j.colsurfb.2021.111841.

 doi:10.20944/preprints202503.0667.v1

133. Yip, A.M.; Shum, J.; Liu, H.; Zhou, H.; Jia, M.; Niu, N.; Li, Y.; Yu, C.; Lo, K.K. Luminescent Rhenium(I)–Polypyridine Complexes Appended with a Perylene Diimide or Benzoperylene Monoimide Moiety: Photophysics, Intracellular Sensing, and Photocytotoxic Activity. *Chem. Eur. J.* **2019**, *25*, 8970–8974, doi:10.1002/chem.201900345.
134. Song, X.; Liang, C.; Gong, H.; Chen, Q.; Wang, C.; Liu, Z. Photosensitizer-Conjugated Albumin−Polypyrrole Nanoparticles for Imaging-Guided In Vivo Photodynamic/Photothermal Therapy. *Small* **2015**, *11*, 3932–3941, doi:10.1002/smll.201500550.
135. Jang, B.; Park, J.-Y.; Tung, C.-H.; Kim, I.-H.; Choi, Y. Gold Nanorod−Photosensitizer Complex for Near-Infrared Fluorescence Imaging and Photodynamic/Photothermal Therapy *In Vivo*. *ACS Nano* **2011**, *5*, 1086–1094, doi:10.1021/nn102722z.
136. Sun, P.; Wang, X.; Wang, G.; Deng, W.; Shen, Q.; Jiang, R.; Wang, W.; Fan, Q.; Huang, W. A Perylene Diimide Zwitterionic Polymer for Photoacoustic Imaging Guided Photothermal/Photodynamic Synergistic Therapy with Single near-Infrared Irradiation. *J. Mater. Chem. B* **2018**, *6*, 3395–3403, doi:10.1039/C8TB00845K.
137. Sun, P.; Huang, T.; Wang, X.; Wang, G.; Liu, Z.; Chen, G.; Fan, Q. Dynamic-Covalent Hydrogel with NIR-Triggered Drug Delivery for Localized Chemo-Photothermal Combination Therapy. *Biomacromolecules* **2020**, *21*, 556–565, doi:10.1021/acs.biomac.9b01290.
138. Lee, Y.-L.; Chou, Y.-T.; Su, B.-K.; Wu, C.; Wang, C.-H.; Chang, K.-H.; Ho, J.A.; Chou, P.-T. Comprehensive Thione-Derived Perylene Diimides and Their Bio-Conjugation for Simultaneous Imaging, Tracking, and Targeted Photodynamic Therapy. *J. Am. Chem. Soc.* **2022**, *144*, 17249–17260, doi:10.1021/jacs.2c07967.
139. Liu, Z.; Gao, Y.; Jin, X.; Deng, Q.; Yin, Z.; Tong, S.; Qing, W.; Huang, Y. Regioisomer-Manipulating Thio-Perylenediimide Nanoagents for Photothermal/Photodynamic Theranostics. *J. Mater. Chem. B* **2020**, *8*, 5535–5544, doi:10.1039/D0TB00566E.
140. Llewellyn, B.A.; Davies, E.S.; Pfeiffer, C.R.; Cooper, M.; Lewis, W.; Champness, N.R. Thionated Perylene Diimides with Intense Absorbance in the Near-IR. *Chem. Commun.* **2016**, *52*, 2099–2102, doi:10.1039/C5CC09962E.